5-2016

Developing Synthetic Methods to Prepare Discrete Metal-Organic Nanotubes

Derek L. Mull
University of Tennessee - Knoxville, dmull@vols.utk.edu

To the Graduate Council:

I am submitting herewith a thesis written by Derek L. Mull entitled "Developing Synthetic Methods to Prepare Discrete Metal-Organic Nanotubes." I have examined the final electronic copy of this thesis for form and content and recommend that it be accepted in partial fulfillment of the requirements for the degree of Master of Science, with a major in Chemistry.

David M. Jenkins, Major Professor

We have read this thesis and recommend its acceptance:

Mark D. Dadmun, Claudia J. Rawn, Michael D. Best

Accepted for the Council:
Carolyn R. Hodges

Vice Provost and Dean of the Graduate School

(Original signatures are on file with official student records.)

Developing Synthetic Methods to Prepare Discrete Metal-Organic Nanotubes

A Thesis Presented for the
Master of Science
Degree
The University of Tennessee, Knoxville

Derek L. Mull
May 2016

DEDICATION

I would like to dedicate this thesis to my high school science teacher, Ms. Michelle Engel. It was she who inspired me to pursue science after high school.

ACKNOWLEDGEMENTS

I'd like to first thank my advisor, Dr. David Jenkins, for his support and encouragement at every step of my graduate career. I have had the fortune to have numerous mentors during my tenure in academia, but I would not be the scientist I am today without his mentorship. I also thank him for all the group socials, they are truly one of a kind. I would like to thank Dr. Shawn Campagna for teaching me almost everything I know about organic chemistry, and I am especially grateful for his patience with my poor background in the subject.

I must thank Dr. Alan Cramer and Dr. Christopher Murdock for the conversations, help, advice, and laughter during my first year, and Dr. Brianna Hughes for being my go-to for questions and help after their departure. To Preeti Chandrachud, my graduate career would not be the same without you. I value our friendship, the coffee breaks, and bouncing ideas off each other, and of course, the column troubleshooting advice. To Maggie Lookadoo, our late night breaks helped me get through the rough times of graduate school and I missed them dearly after you left. To the rest of the Jenkins group, thank you for your support, encouragement, and for tolerating my moods.

ABSTRACT

Metal-organic nanotubes (MONTs) are an emerging class of discrete materials that are the 1D variant of metal-organic frameworks (MOFs). MONTs have potential to become an alternative 1D material to carbon nanotubes, metal oxide nanotubes, and boron nitride nanotubes because they possess an organic ligand that can be functionalized and tuned for specific applications. Despite this potential, only a handful of structures have been reported and only two examples of discrete MONTs exist in the literature. It is thus imperative to develop general methods to prepare and characterize discrete MONTs to bring them to the forefront of the scientific literature.

Efforts were directed to design ligands that will readily facilitate MONT dispersion post-synthetically, or by hindering their crystal packing as they form from solution. Our group has previously reported 5 MONT structures that employ semi-rigid, di-triazole ligands, and by employing isoreticular synthesis, our goal was to determine which structural characteristics will direct MONTs to form discrete nanotubes or small bundles. A collaboration with the Dadmun group here at UTK was established to employ small-angle scattering methods to study their kinetics and growth, information that will be useful to guide future efforts to prepare discrete MONTs.

TABLE OF CONTENTS

LIST OF TABLES

LIST OF FIGURES

LIST OF SCHEMES

CHAPTER 1
INTRODUCTION

The field of one dimensional materials ignited with the discovery of carbon nanotubes (CNTs) in 1991.[1] Since then, both single-walled and multi-walled CNTs (SWCNT/MWCNT),[1-2] boron nitride nanotubes,[3] numerous metal oxide nanotubes,[4] and peptide-based biological nanotubes have been reported.[5] As seen in carbon nanotubes, reducing the dimensionality of a material, from its 3D bulk phase, to a 2D or 1D variant can drastically alter its properties. Indeed, low dimensional materials could revolutionize computing and electronics, medicine, and commercial products because of changes in electronic and tensile properties as the dimensions are reduced.[6]

Metal-organic nanotubes (MONTs) are the 1D variant of metal-organic frameworks (MOFs), a class of materials that entered the forefront of the scientific literature in the early 2000s. MOFs are crystalline, highly porous materials that can act as molecular sponges and possess far-reaching applications in gas storage,[7] CO_2 sequestration,[8] fuel cells for vehicular applications,[9] heterogeneous catalysis,[10] and separations.[11] Because MONTs and MOFs are synthesized from metal salts and organic linkers, often under solvothermal conditions, thousands of combinations are possible, and indeed thousands of 3D MOFs have been reported.[12] While 2D MOFs number in the hundreds,[13] MONTs remain a relatively uncharted among the world of low dimensional materials.[14]

Back in the early 2000s, Yaghi and coworkers pioneered the now well established principle of isoreticularity (see Figure 1.1), where two MOFs alter in pore size, metal, or chemical functionality but possess the same pore topology.[15] This key feature is what sparked interest in MOFs over the last 16 years and is precisely what makes MONTs an

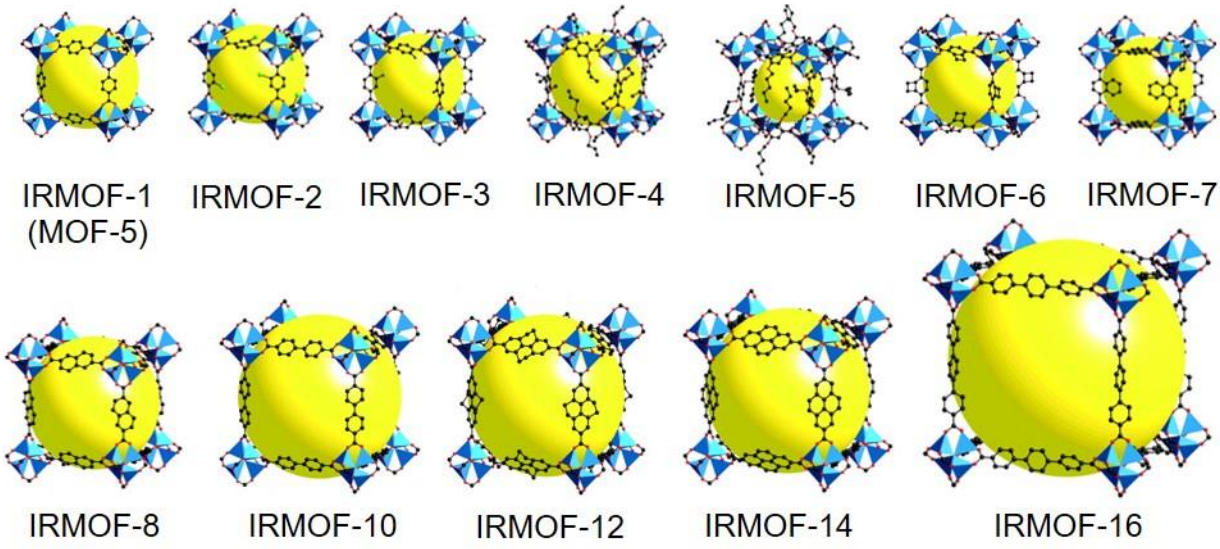

Figure 1.1: First isostructural MOFs synthesized in 2002 by Yaghi and coworkers. The authors demonstrated that both size and the chemical environment of the pore can be systematically altered by adjusting the ligand of the parent MOF, MOF-5.[15b]

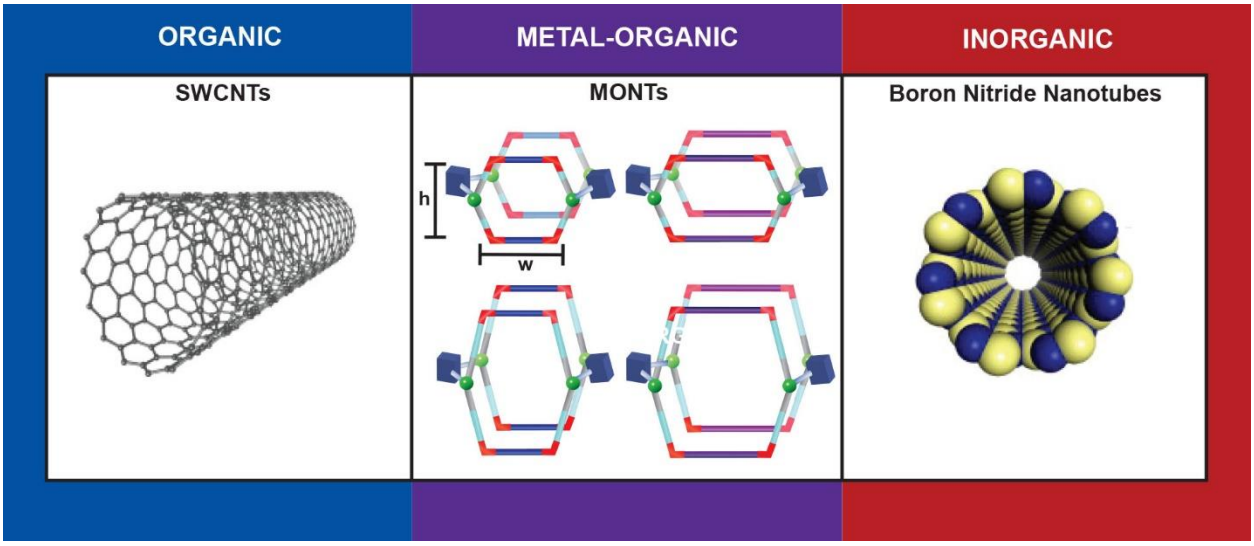

Figure 1-2. Metal-organic nanotubes are the 1D variant of MOFs whose chemical tunability offers a distinct advantage over their purely organic and inorganic counterparts.

attractive alternative to their purely organic and inorganic counterparts (Figure 1.2). Control over pore size and chemical functionalization is limited for SWCNTS, and they require energy intensive methods to prepare, can be difficult to purify, often with low yields, and are expensive.[16] MONTs have been synthesized under solvothermal conditions and at room temperature, and our group has been able to demonstrate isostructural synthesis of porous MONTs.[17]

MONTs can form via a curling up mechanism, where the metal and ligand form linear chains that curl around each other to form a tube; via the two-column approach where a semi-rigid ligand adopts a *syn* formation and the metal forms down the length of the tube; via a four column approach where rigid, linear linkers bind to the metal and a capping ligand binds to the periphery; and via a greater than four column approach in which small, rigid/semi-rigid linkers form a metallomacrocycle that stacks into the tube. These four approaches can be visualized in Figure 1.3.

One of the earliest MONT structures was reported by Sun and coworkers in 2008.[18] The structure was prepared from 5-amino-2,4,6-triiodoisophthalic acid, 4,4'-bipyridine, and zinc nitrate hexahydrate in a DMF, ethanol, and water solvent system to form a 4-column pillar nanotube. Since then, approximately 40 structures have been synthesized by various groups around the world from a variety of ligands, metal sources, and reaction conditions. As mentioned previously, the majority of MONTs are prepared under solvothermal conditions, but a few have been synthesized at room temperature by simple crystallization techniques. For example, a MONT prepared by Forbes and coworkers was synthesized from uranyl nitrate, iminodiacetic acid and piperazine in a 1:1 water:methanol

combination by crystallization over 3 d.[19] Hexagonal macrocycles crystallized into a corrugated nanotube structure in which confined ice channels were crystallographically observed within the pore of the tube.[19]

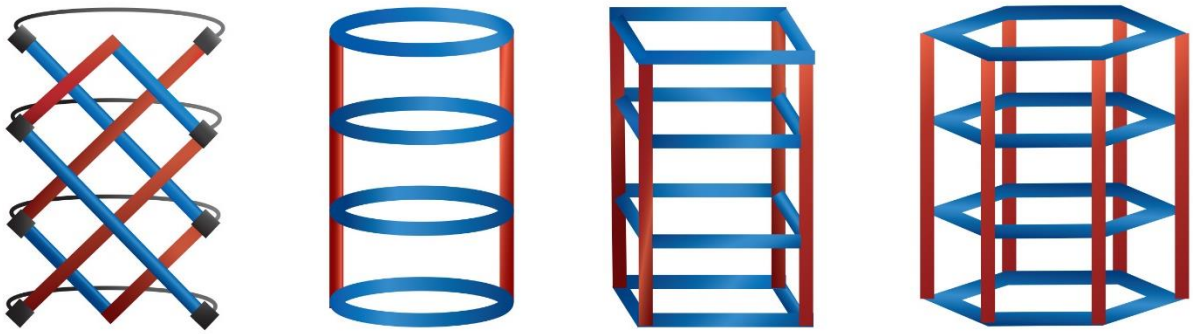

Figure 1.3. MONTs can form in four ways: through a curling-up mechanism (A), a 2-column pillar approach (B), a 4-column pillar approach (C), or a greater than 4-column approach (D). A cartoon of a 6-pillar structure is shown here.

An approach was utilized by Kitagawa and coworkers in which platinum nitrate was reacted with 4,4'-bipy and ethylenediamine to form a metallomacrocycle, and upon oxidative polymeriazation with I_2, the material crystalized into a four-column MONT held together by bridging iodides.[20] The nanotubes formed were discrete, albeit packed into a 3D crystalline lattice. The authors were able to prepare nanotubes with bridging bromides and chlorides through the same oxidative polymerization step and it was found that the lowest energy structure was indeed the MONT with the bridging iodide.[20]

Our group was the first to apply the principles of isoreticular synthesis to that of MONTs.[17] Five MONT structures were prepared from silver nitrate, copper (II) bromide,

or copper (II) sulfate with semi-rigid, 1,2,4-ditriazole ligands of increasing length. The ligands possessed an aryl backbone and two points of rotation in the form of methylene bridges between the aryl and 1,2,4-triazole units, and it was this property that allowed the ligands to adopt a *syn* conformation to form nanotubes. Each structure possessed bridging anions, either nitrates, bromides, or sulfates, that formed the bases of 1D connectivity. The packing of these nanotubes into 3D crystalline lattices was driven by π-π stacking of the aromatic units of the ligands.

Though each of these structures described formed individual tubes that were packed in 3D, not all structures reported as metal-organic nanotubes are actually discrete nanotubes. Several structures in the literature can be more aptly described as 3D or 2D MOFs with 1D pores rather than packed metal-organic nanotubes (Figure 1.4). However, even those structures that are individual tubes, their 3D packing is a limiting factor for the development of MONTs as a highly anisotropic, 1D material. *Indeed, until they can effectively be dispersed to their discrete, non-packed form, MONTs are effectively the same as MOFs.*

The Aida group at the University of Tokyo managed to prepare two discrete nanotubes from ferrocene-derived tetra-pyridyl ligands.[21] The ligands bind to Ag to form large metallomacrocycles which form free-flowing, 10-column nanotubes by π-π stacking of the ligands. These tubes, however, do not have the covalent bonds of MONTs. The tubes were not packed in 3D and were characterized by transmission electron microscopy (TEM) and atomic force microscopy (AFM) and are shown in Figure 1.5. The redox-active ferrocene group incorporated into the ligands allowed for oxidative cutting of the

nanotubes to their constituent nanorings, and the tubes could be reassembled upon reduction.[21] The group was able to follow up this study with the preparation of isoreticular nanotubes in which chiral substituents were incorporated onto the ligand.[22] While these exotic structures demonstrate that a free-flowing, 1D material comprised entirely of coordination bonds and π-π stacking is possible, there is some contention as to whether or not it is a true MONT due to the fact that metal chains that are a common feature in MOFs and other MONTs are notably absent.

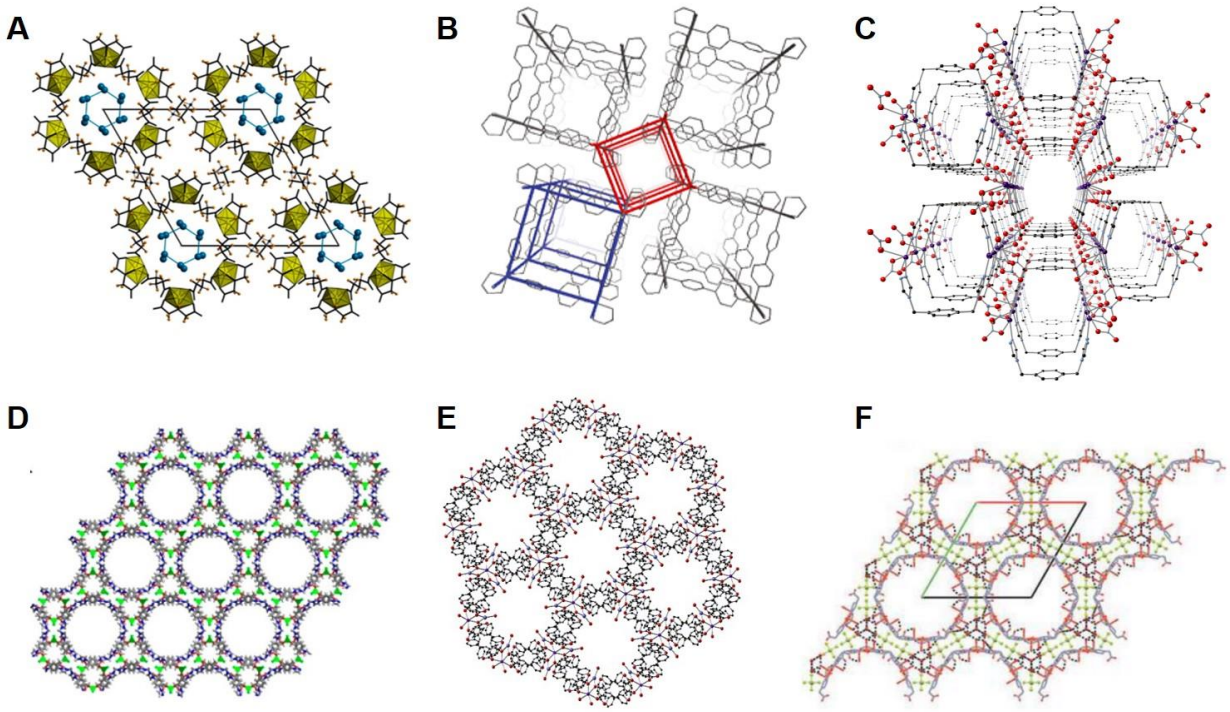

Figure 1.4. MONTs packed into 3D crystalline lattices (A-C). Some MONT structures reported are more structurally analogous to 2D and 3D MOFs with 1D pores (D-F). These images are modified from the original references.[17, 19-20, 23]

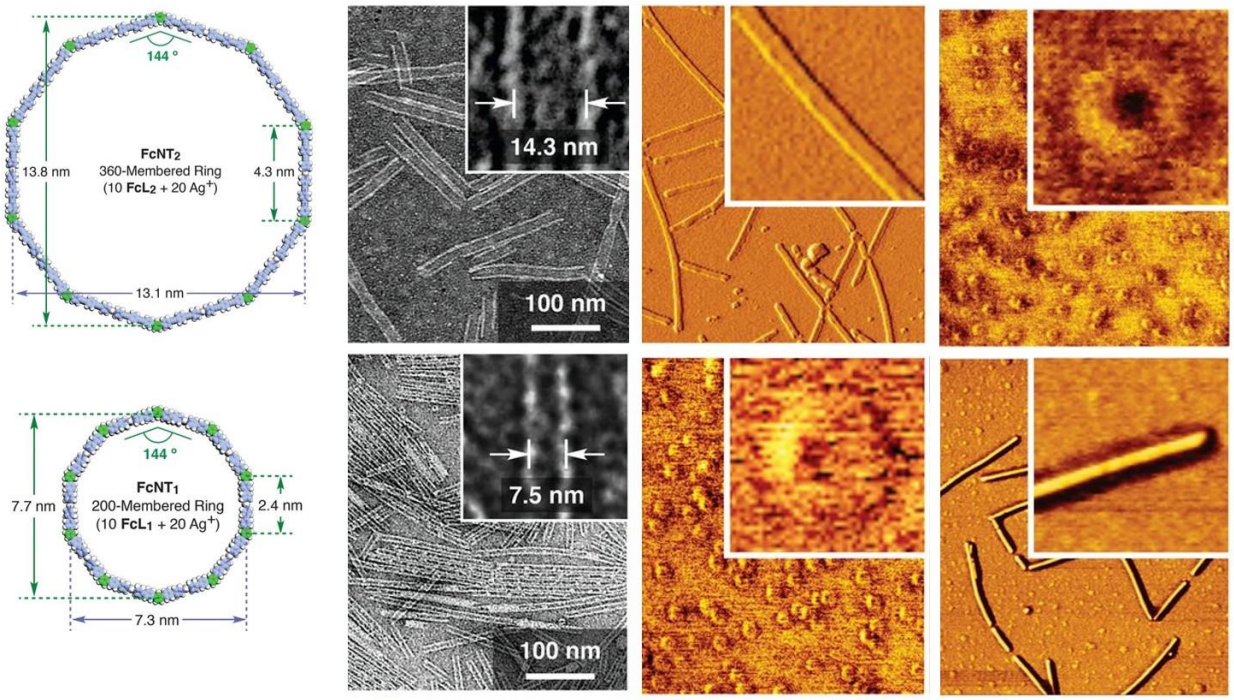

Figure 1.5. Proposed structures, TEM, and AFM images of two nanotubes synthesized by Aida and coworkers. The black and white images are TEM micrographs of each nanotube, and the AFM images (colored orange) show the constituent nanorings after oxidative cutting. These images are modified from the original reference.[21]

The diversity of the structures discussed here underscore the large potential of MONTs despite the fact that relatively few structures have been reported. Harnessing the properties of these 1D materials require the need to develop generalizable methods that will allow researchers to bring MONTs into the mainstream of materials science. One critical consideration is the development of methods to characterize MONTs once they have been dispersed to their discrete state. While electron microscopy can offer high resolution images, not all materials are stable under an electron beam, and degradation can occur before an image can be obtained. Indirect routes to characterize discrete materials are thus necessary to explore and define in such a way that can be applied generally to the host of MONT structures that are possible.

This thesis describes efforts undertaken to reduce the crystallite size of MONTs, both post-synthetically and through the design of ligands that may prevent the tubes from aggregating as they form. Initial work was carried out to disperse a previously published silver MONT structure synthesized in the Jenkins group, but the focus later shifted to designing ligands that would reduce the π-π stacking of the nanotubes as they formed. Our group established a collaboration with the Dadmun group to employ small-angle scattering methods to better understand how MONTs nucleate and grow in order to guide how to better design future materials.

References

1. Iijima, S., Helical microtubules of graphitic carbon. *Nature* **1991,** *354*, 56-58.
2. Iijima, S.; Ichihashi, T., Single-shell carbon nanotubes of 1-nm diameter. *Nature* **1993,** *363*, 603-605.
3. (a) Golberg, D.; Bando, Y.; Tang, C. C.; Zhi, C. Y., Boron Nitride Nanotubes. *Adv. Mater.* **2007,** *19*, 2413-2432; (b) Wang, J.; Lee, C. H.; Yap, Y. K., Recent advancements in boron nitride nanotubes. *Nanoscale* **2010,** *2*, 2028-2034; (c) Zhi, C.; Bando, Y.; Tang, C.; Golberg, D., Boron nitride nanotubes. *Mat. Sci. Eng. R* **2010,** *70*, 92-111.
4. (a) Devan, R. S.; Patil, R. A.; Lin, J.-H.; Ma, Y.-R., One-Dimensional Metal-Oxide Nanostructures: Recent Developments in Synthesis, Characterization, and Applications. *Adv. Funct. Mater.* **2012,** *22*, 3326-3370; (b) Lee, M.; Kim, T.; Bae, C.; Shin, H.; Kim, J., Fabrication and applications of metal-oxide nano-tubes. *JOM* **2010,** *62*, 44-49; (c) Li, Y.; Yang, X.-Y.; Feng, Y.; Yuan, Z.-Y.; Su, B.-L., One-Dimensional Metal Oxide Nanotubes, Nanowires, Nanoribbons, and Nanorods: Synthesis, Characterizations, Properties and Applications. *Crit. Rev. Solid State Mater. Sci.* **2012,** *37*, 1-74.
5. (a) Cenker, Ç. Ç.; Bomans, P. H. H.; Friedrich, H.; Dedeoğlu, B.; Aviyente, V.; Olsson, U.; Sommerdijk, N. A. J. M.; Bucak, S., Peptide nanotube formation: a crystal growth process. *Soft Matter* **2012,** *8*, 7463-7470; (b) Graveland-Bikker, J. F.; Fritz, G.; Glatter, O.; De Kruif, C. G., Growth and structure of α-lactalbumin nanotubes. *J. Appl. Crystallogr.* **2006,** *39*, 180-184; (c) Kapil, N.; Singh, A.; Singh, M.; Das, D., Efficient MoS2 Exfoliation by Cross-β-Amyloid Nanotubes for Multistimuli-Responsive and Biodegradable Aqueous Dispersions. *Angew. Chem.* **2016**, ASAP; (d) Thomas, F.; Burgess, N. C.; Thomson, A. R.; Woolfson, D. N., Controlling the Assembly of Coiled–Coil Peptide Nanotubes. *Angew. Chem. Int. Ed.* **2016,** *55*, 987-991.
6. Odom, T. W.; Huang, J.-L.; Kim, P.; Lieber, C. M., Atomic structure and electronic properties of single-walled carbon nanotubes. *Nature* **1998,** *391*, 62-64.
7. (a) Cui, Y.; Li, B.; He, H.; Zhou, W.; Chen, B.; Qian, G., Metal–Organic Frameworks as Platforms for Functional Materials. *Acc. Chem. Res.* **2016,** *49*, 483-493; (b) Li, J.-R.; Ma, Y.; McCarthy, M. C.; Sculley, J.; Yu, J.; Jeong, H.-K.; Balbuena, P. B.; Zhou, H.-C., Carbon dioxide capture-related gas adsorption and separation in metal-organic frameworks. *Coord. Chem. Rev.* **2011,** *255*, 1791-1823.
8. (a) Bhattacharya, B.; Ghoshal, D., Selective carbon dioxide adsorption by mixed-ligand porous coordination polymers. *CrystEngComm* **2015,** *17*, 8388-8413; (b) Liu, Y.; Yang, Y.; Sun, Q.; Wang, Z.; Huang, B.; Dai, Y.; Qin, X.; Zhang, X., Chemical Adsorption Enhanced CO2 Capture and Photoreduction over a Copper Porphyrin Based Metal Organic Framework. *ACS Appl. Mater. Interfaces* **2013,** *5*, 7654-7658; (c) Martínez, F.; Sanz, R.; Orcajo, G.; Briones, D.; Yángüez, V., Amino-impregnated MOF materials for CO2 capture at post-combustion conditions. *Chem. Eng. Sci.* **2016,** *142*, 55-61.
9. (a) Ma, S.; Meng, L., Energy-related applications of functional porous metal–organic frameworks. In *Pure Appl. Chem.*, **2010**, *83*, 167; (b) Ren, Y.; Chia, G. H.; Gao, Z.,

Metal–organic frameworks in fuel cell technologies. *Nano Today* **2013,** *8*, 577-597; (c) Yoon, M.; Suh, K.; Natarajan, S.; Kim, K., Proton Conduction in Metal–Organic Frameworks and Related Modularly Built Porous Solids. *Angew. Chem. Int. Ed.* **2013,** *52*, 2688-2700.

10. (a) Furukawa, H.; Cordova, K. E.; O'Keeffe, M.; Yaghi, O. M., The Chemistry and Applications of Metal-Organic Frameworks. *Science* **2013,** *341*, 974; (b) Kuppler, R. J.; Timmons, D. J.; Fang, Q.-R.; Li, J.-R.; Makal, T. A.; Young, M. D.; Yuan, D.; Zhao, D.; Zhuang, W.; Zhou, H.-C., Potential applications of metal-organic frameworks. *Coord. Chem. Rev.* **2009,** *253*, 3042-3066.
11. (a) Heinke, L.; Tu, M.; Wannapaiboon, S.; Fischer, R. A.; Wöll, C., Surface-mounted metal-organic frameworks for applications in sensing and separation. *Microporous Mesoporous Mater.* **2015,** *216*, 200-215; (b) Krishna, R., Methodologies for evaluation of metal-organic frameworks in separation applications. *RSC Adv.* **2015,** *5*, 52269-52295; (c) Li, S.; Yang, K.; Tan, C.; Huang, X.; Huang, W.; Zhang, H., Preparation and applications of novel composites composed of metal-organic frameworks and two-dimensional materials. *Chem. Commun.* **2016,** *52*, 1555-1562; (d) Yeo, Z. Y.; Chai, S.-P.; Zhu, P. W.; Mohamed, A. R., An overview: synthesis of thin films/membranes of metal organic frameworks and its gas separation performances. *RSC Adv.* **2014,** *4*, 54322-54334.
12. (a) Cai, S.-L.; Zheng, S.-R.; Fan, J.; Zeng, R.-H.; Zhang, W.-G., Two new three-dimensional metal-organic frameworks with 4-connected diamondoid and unusual (6,16)-connected net topologies based on planar tetranuclear squares as secondary building units. *CrystEngComm* **2016,** *18*, 1174-1183; (b) Carlucci, L.; Ciani, G.; Maggini, S.; Proserpio, D. M.; Visconti, M., Heterometallic Modular Metal–Organic 3D Frameworks Assembled via New Tris-β-Diketonate Metalloligands: Nanoporous Materials for Anion Exchange and Scaffolding of Selected Anionic Guests. *Chem. Eur. J.* **2010,** *16*, 12328-12341; (c) Jeong, S.; Kim, D.; Shin, S.; Moon, D.; Cho, S. J.; Lah, M. S., Combinational Synthetic Approaches for Isoreticular and Polymorphic Metal–Organic Frameworks with Tuned Pore Geometries and Surface Properties. *Chem. Mater.* **2014,** *26*, 1711-1719; (d) Li, H.; Eddaoudi, M.; O'Keeffe, M.; Yaghi, O. M., Design and synthesis of an exceptionally stable and highly porous metal-organic framework. *Nature* **1999,** *402*, 276-279; (e) Tan, X.; Li, L.; Zhang, J.; Han, X.; Jiang, L.; Li, F.; Su, C.-Y., Three-Dimensional Phosphine Metal–Organic Frameworks Assembled from Cu(I) and Pyridyl Diphosphine. *Chem. Mater.* **2012,** *24*, 480-485; (f) Wang, J.; Zhang, Y.-H.; Tong, M.-L., Two new 3D metal-organic frameworks of nanoscale cages constructed by Cd(ii) and conformationally-flexible cyclohexanehexacarboxylate. *Chem. Commun.* **2006**, 3166-3168.
13. (a) Campbell, M. G.; Liu, S. F.; Swager, T. M.; Dincă, M., Chemiresistive Sensor Arrays from Conductive 2D Metal–Organic Frameworks. *J. Am. Chem. Soc.* **2015,** *137*, 13780-13783; (b) Liu, H.; Li, X.; Chen, L.; Wang, X.; Pan, H.; Zhang, X.; Zhao, M., Gas Adsorption Effects on the Electronic Properties of Two-Dimensional Nickel Bis(dithiolene) Complex. *J. Phys. Chem. C* **2016,** *120*, 3846-3852; (c) Murdock, C. R.; McNutt, N. W.; Keffer, D. J.; Jenkins, D. M., Rotating Phenyl Rings as a Guest-

Dependent Switch in Two-Dimensional Metal–Organic Frameworks. *J. Am. Chem. Soc.* **2014,** *136*, 671-678.
14. Thanasekaran, P.; Luo, T.-T.; Lee, C.-H.; Lu, K.-L., A journey in search of single-walled metal-organic nanotubes. *J. Mater. Chem.* **2011,** *21*, 13140-13149.
15. (a) Deng, H.; Grunder, S.; Cordova, K. E.; Valente, C.; Furukawa, H.; Hmadeh, M.; Gándara, F.; Whalley, A. C.; Liu, Z.; Asahina, S.; Kazumori, H.; O'Keeffe, M.; Terasaki, O.; Stoddart, J. F.; Yaghi, O. M., Large-Pore Apertures in a Series of Metal-Organic Frameworks. *Science* **2012,** *336*, 1018-1023; (b) Eddaoudi, M.; Kim, J.; Rosi, N.; Vodak, D.; Wachter, J.; O'Keeffe, M.; Yaghi, O. M., Systematic Design of Pore Size and Functionality in Isoreticular MOFs and Their Application in Methane Storage. *Science* **2002,** *295*, 469-472.
16. (a) Ameen, A. A.; Giordano, A. N.; Alston, J. R.; Forney, M. W.; Herring, N. P.; Kobayashi, S.; Ridlen, S. G.; Subaran, S. S.; Younts, T. J.; Poler, J. C., Aggregation kinetics of single-walled carbon nanotubes investigated using mechanically wrapped multinuclear complexes: probing the tube-tube repulsive barrier. *Phys. Chem. Chem. Phys.* **2014,** *16*, 5855-5865; (b) Azoz, S.; Gilbertson, L. M.; Hashmi, S. M.; Han, P.; Sterbinsky, G. E.; Kanaan, S. A.; Zimmerman, J. B.; Pfefferle, L. D., Enhanced dispersion and electronic performance of single-walled carbon nanotube thin films without surfactant: A comprehensive study of various treatment processes. *Carbon* **2015,** *93*, 1008-1020; (c) Forney, M. W.; Poler, J. C., Significantly Enhanced Single-Walled Carbon Nanotube Dispersion Stability in Mixed Solvent Systems. *J. Phys. Chem. C* **2011,** *115*, 10531-10536; (d) Koh, B.; Cheng, W., The Impact of Sonication on the Surface Quality of Single-Walled Carbon Nanotubes. *J. Pharm. Sci.* **2015,** *104*, 2594-2599.
17. Murdock, C. R.; Jenkins, D. M., Isostructural Synthesis of Porous Metal–Organic Nanotubes. *J. Am. Chem. Soc.* **2014,** *136*, 10983-10988.
18. Dai, F.; He, H.; Sun, D., A Metal−Organic Nanotube Exhibiting Reversible Adsorption of $(H_2O)_{12}$ Cluster. *J. Am. Chem. Soc.* **2008,** *130*, 14064-14065.
19. Unruh, D. K.; Gojdas, K.; Libo, A.; Forbes, T. Z., Development of Metal–Organic Nanotubes Exhibiting Low-Temperature, Reversible Exchange of Confined "Ice Channels". *J. Am. Chem. Soc.* **2013,** *135*, 7398-7401.
20. Otsubo, K.; Wakabayashi, Y.; Ohara, J.; Yamamoto, S.; Matsuzaki, H.; Okamoto, H.; Nitta, K.; Uruga, T.; Kitagawa, H., Bottom-up realization of a porous metal–organic nanotubular assembly. *Nat. Mater.* **2011,** *10*, 291-295.
21. Fukino, T.; Joo, H.; Hisada, Y.; Obana, M.; Yamagishi, H.; Hikima, T.; Takata, M.; Fujita, N.; Aida, T., Manipulation of Discrete Nanostructures by Selective Modulation of Noncovalent Forces. *Science* **2014,** *344*, 499-504.
22. Yamagishi, H.; Fukino, T.; Hashizume, D.; Mori, T.; Inoue, Y.; Hikima, T.; Takata, M.; Aida, T., Metal–Organic Nanotube with Helical and Propeller-Chiral Motifs Composed of a C10-Symmetric Double-Decker Nanoring. *J. Am. Chem. Soc.* **2015,** *137*, 7628-7631.
23. (a) Adarsh, N. N.; Dîrtu, M. M.; Naik, A. D.; Léonard, A. F.; Campagnol, N.; Robeyns, K.; Snauwaert, J.; Fransaer, J.; Su, B. L.; Garcia, Y., Single-Walled Metal–Organic Nanotube Built from a Simple Synthon. *Chem. Eur. J.* **2015,** *21*, 4300-4307; (b) Kong,

G.-Q.; Ou, S.; Zou, C.; Wu, C.-D., Assembly and Post-Modification of a Metal–Organic Nanotube for Highly Efficient Catalysis. *J. Am. Chem. Soc.* **2012,** *134*, 19851-19857; (c) Luo, T.-T.; Wu, H.-C.; Jao, Y.-C.; Huang, S.-M.; Tseng, T.-W.; Wen, Y.-S.; Lee, G.-H.; Peng, S.-M.; Lu, K.-L., Self-Assembled Arrays of Single-Walled Metal–Organic Nanotubes. *Angew. Chem. Int. Ed.* **2009,** *48*, 9461-9464.

CHAPTER 2
DEVELOPING METHODS TO PREPARE AND CHARACTERIZE DISCRETE METAL-ORGANIC NANOTUBES

Part of the work detailed in this chapter was originally published by Thusitha Etampawala, Derek L. Mull, Jong. K. Keum, David M. Jenkins, and Mark Dadmun:

Thusitha Etampawala, Derek L. Mull, Jong. K. Keum, David M. Jenkins, and Mark Dadmun "Insights into the Morphology and Kinetics of Growth of Silver Metal-Organic Nanotubes." *Cryst. Growth Des.* **2016**, *16*, 1395-1403.

All work presented here was carried out with assistance of Guoliang Li, Ondrej Dyck, and Thusitha Etampawala.

Abstract

The preparation of discrete metal-organic nanotubes (MONTs) is currently under investigation by a handful of research groups across the globe. The vast majority of structures published to date are packed into 3D crystalline lattices limiting their applications as highly anisotropic 1D materials. It is thus imperative to develop methods to prepare discrete MONTs *in situ* or post-synthetically. The studies discussed in this chapter are preliminary investigations toward MONT dispersion and of the mechanism of MONT formation and aggregation.

Introduction

Discrete, one-dimensional materials have been intensively studied since the discovery of multi-walled carbon nanotubes (MWCNTs) in 1991,[1] and single-walled carbon nanotubes (SWCNTs) were first described in 1993.[2] SWCNTs are highly attractive

materials because they possess outstanding tensile strength[3] and can be either metallic or semiconducting depending upon the chirality (or angle of propagation of carbon atoms) of the tube. These conductive properties stem from the fact that all the carbon atoms are sp^2-hybridized, which allows for charge delocalization down the length of the tube.[4]

The most common synthetic routes, which include arc discharge, laser ablation, and high-pressure carbon monoxide disproportionation, leave a mixture of carbonaceous products that require further purification.[5] Once purified, it is necessary to disperse SWCNTs to their discrete form, a process that is typically carried out in solution. This is often hindered by poor solubility due to the tendency to aggregate by π-π stacking, and SWCNT dispersion often occurs in low yields.[5b, 5c] Surfactants can be added to solution in order to increase SWCNT solubility, but surfactant and solvent residues on the nanotube surface can impede performance.[6] Methods have been developed to grow vertically aligned forests of SWCNTs but these are energy intensive and expensive.[7] Low temperature routes to prepare highly anisotropic 1D materials and 1D materials with useful electronic properties are an attractive route to overcome the cost and energy limitations of SWCNTs.

Metal-Organic Nanotubes (MONTs) are an inorganic-organic hybrid material that are prepared under solvothermal conditions from organic ligands and metal salt precursors, and are structural analogous to SWCNTs.[8] MONTs offer an attractive alternative to SWCNTs and their inorganic counterparts[9] because the size and elemental composition can be readily tuned by simply adjusting the organic ligand and metal salt. The 1D variant of metal-organic frameworks (MOFs), MONTs aggregate into a bulk

crystalline phase when they form from solution. The aggregation of MONTs is typically driven by π-π stacking of aromatic ligands, although hydrogen-bonded MONTs have also been reported.[10] Because all but one example[11] of MONTs prepared to date are packed into a crystalline lattice, they are effectively the same as 3D MOFs and thus it is necessary to devise methods to reduce crystallite size either *in situ* or through post-synthetic modification (PSM) to prepare discrete, anisotropic 1D nanotubes.

Our group previously reported the first series of isostructural, porous MONTs that were published in *J. Am. Chem. Soc.* in 2014 (Fig. 2.1).[12] The nanotubes in each of the five structures were aggregated in 3D due to π-π stacking from the aromatic moieties within the ligand. The metal centers were capped with either sulfate anions, nitrate anions, or bridging halides, all of which bind weakly to the metal. This structural feature provides the additional challenge of maintaining the structural integrity of the nanotubes while attempting dispersion with post-synthetic methods. Our initial investigations into MONT dispersion focused on post-synthetic reduction of crystallite size using mechanical force.

Results and Discussion

Initial attempts to disperse the MONTs were carried out with two of the five in the series (Fig. 2.1), $[Ag_2(\mathbf{1})(NO_3)_2]\cdot$NMP and $[Cu_2(\mathbf{1})(Br)_2]\cdot$DMF MONTs prepared from the *para*-xyly ditriazole ligand 1,4-bis(4-(4H-1,2,4-triazol-4-yl)benzyl)benzene (**1**) (Fig. 2.1). Numerous reports of SWCNT dispersion using a probe sonicator[5d] led us to employ the

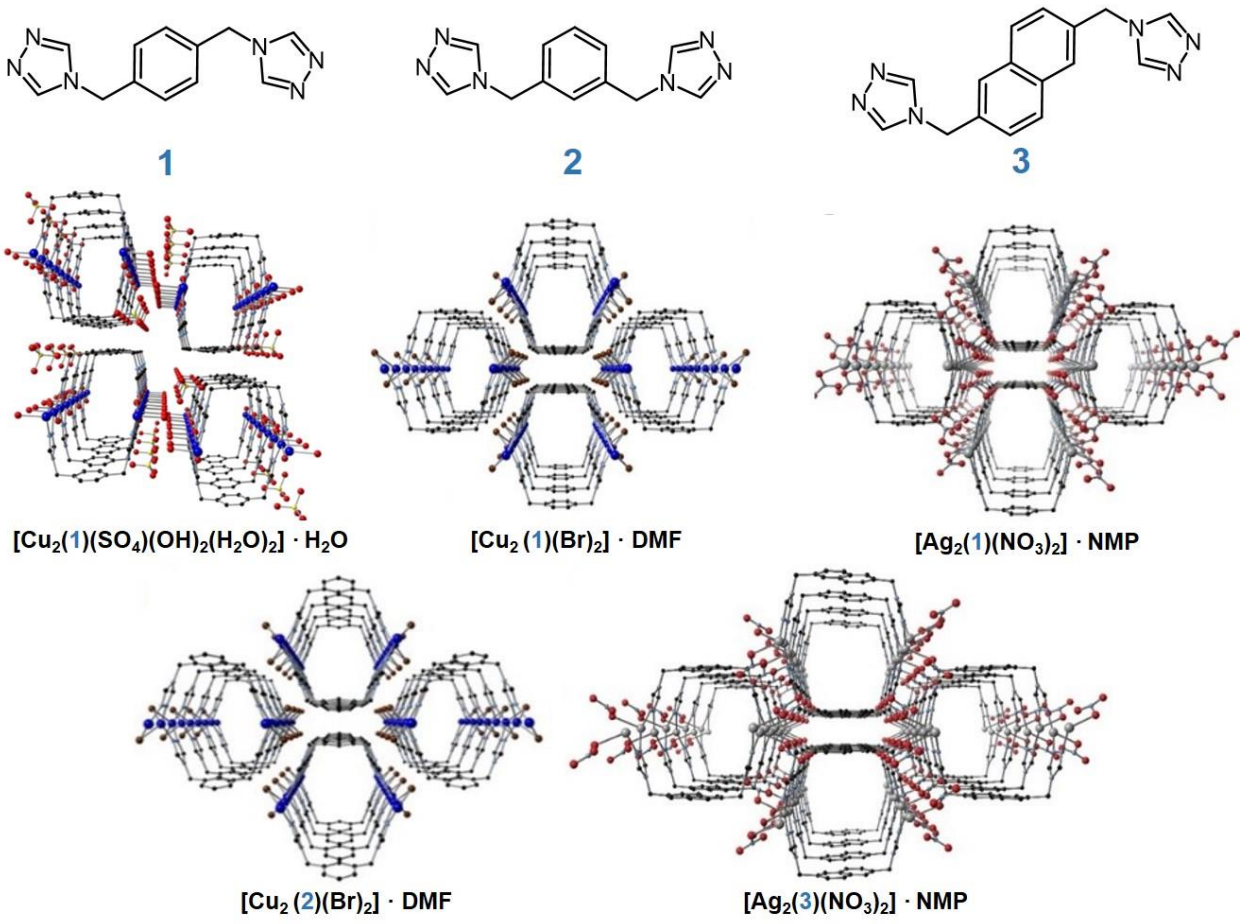

Figure 2.1. Five isostructural metal-organic nanotubes synthesized by Christopher Murdock. Altering the ligand allowed the pore width to be tuned in each of the structures.[12]

bath sonicator available in our laboratory. The bath sonicator operates at a much lower frequency than a probe sonicator, a feature that is better suited for MONT dispersion due to the far weaker bonds that hold the nanotube together. Characterization of the dispersity of MONTs was attempted using a transmission electron microscope (TEM) in the microscopy facilities at the University of Tennessee with assistance from Guoliang Li in the Camden group prior to Dr. Camden's move to the University of Notre Dame.

The samples were immersed in 2 mL methanol prior and sonicated for 30 seconds before pipetting the suspension on a TEM grid, which were then dried overnight prior to analysis. Unfortunately, samples were amorphized under the electron beam, and the micrographs showed Ag nanoparticles of two different size ranges. The large Ag nanoparticles are likely side products from the MONT reactions whereas the small nanoparticles could have formed after sonication or exposure to the electron beam.

To investigate whether these formed from the electron beam or from sonication prior to loading sample onto the graphite grid, the effect of sonication on both the $[Ag_2(\mathbf{1})(NO_3)_2]\cdot$NMP and $[Cu_2(\mathbf{1})(Br)_2]\cdot$DMF were investigated at times of 5 s, 10 s, 30 s, 1 min, 5 min, 10 min, and 30 min (Fig. 2.2). Sonication appeared to caused immediate degradation in $[Cu_2(\mathbf{1})(Br)_2]\cdot$DMF as sonication for as little as 5 seconds causes the disappearance of a majority of peak intensities in all of the diffraction patterns. Sonication of $[Ag_2(\mathbf{1})(NO_3)_2]\cdot$NMP appeared to cause less degradation to the MONT structure as many of the peak intensities were observed after sonication for 30 min. An additional low angle peak did appear after sonication for as little as 5 s, and the baseline noise indicates loss of crystallinity in the structure. Whether this is due to dispersion or sample

degradation remains unclear, but indicates a greater robustness of the $[Ag_2(\mathbf{1})(NO_3)_2]\cdot$NMP sample.

Two follow up studies were carried out with assistance from Ondrej Dyck of the Duscher group in Materials Science and Engineering at UTK. Because the size of the nanotubes pushed the resolution limit of the microscopes available to us (ca. 0.1 nm), our goal was to determine which conditions we could image the crystalline MONT samples without sample degradation. Reduction of the beam current to prevent sample amorphization was attempted, but unfortunately the appropriate current to prevent this was too low to obtain a clear image. For the third attempt to characterize $[Ag_2(\mathbf{1})(NO_3)_2]\cdot$NMP by TEM, the sample was stained with uranyl nitrate in methanol overnight prior to loading the sample onto the TEM grid. Under normal TEM conditions, striations were observed, but matching a diffractogram taken of the sample at different orientations revealed the sample was crystallized uranium rather than the MONT sample.

The limitations of employing transmission electron microscopy to characterize the bulk $[Ag_2(\mathbf{1})(NO_3)_2]\cdot$NMP sample required that we develop alternative methods to study discrete MONTs. While sonication of the as-synthesized material could achieve dispersed tubes, it is more likely that this will result in sample degradation. It is therefore necessary to investigate *in situ* methods to directly prepare free-flowing MONTs and employ alternative methods beyond X-ray crystallography to fully characterize nanotubes at the sub-nanometer level.

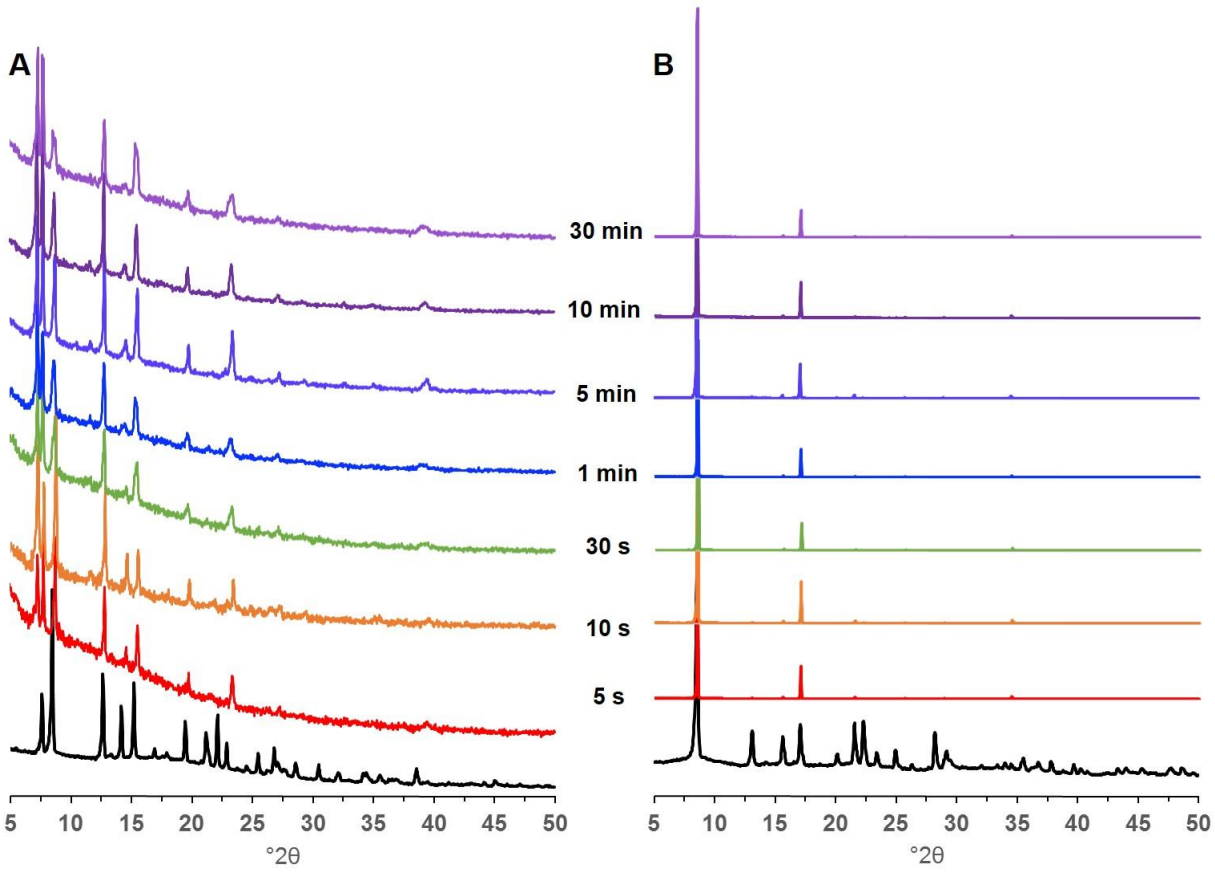

Figure 2.2. Overlay of PXRD patterns after sonication of A) $[Ag_2(1)(NO_3)_2]$·NMP and B) $[Cu_2(1)(Br)_2]$·DMF. The patterns in black indicate the diffraction pattern of the bulk material.

Small-angle X-ray scattering (SAXS) is one method that has been employed to characterize low dimensional materials that are not readily characterized by X-ray crystallography.[13] SAXS has been used to study the growth mechanism and structural features of transition metal chalcogenide nanorods, particularly length and diameter.[14] Employing SAXS to glean a thorough understanding of the growth mechanism will guide researchers to devise methods to inhibit nanotube aggregation to form bulk crystalline material during the course of the reaction. Because SAXS can provide structural information, it can be envisaged that it can also serve to characterize the size and length of the individual nanotubes or nanotube bundles through the course of the reaction.

Our group collaborated with the Dadmun group here at UTK for their expertise in small angle scattering.[15] We selected studying the mechanism of growth for $[Ag_2(\mathbf{1})(NO_3)_2]\cdot$NMP to determine how the nanotubes form and aggregate as the reaction moves toward completion. We hypothesized two possibilities: 1) that the nanotubes formed initially, then aggregated to into the bulk crystalline material as the reaction progressed, or 2) initial nanorings clusters aggregated, then underwent 1D chain growth to form nanotubes later in the reaction.[16]

Experiments were carried out on $[Ag_2(\mathbf{1})(NO_3)_2]\cdot$NMP by Thusitha Etampawala at Oak Ridge National Laboratory and the data were analyzed using the Gualtieri model of nucleation and growth that was developed for the solvothermal synthesis of zeolites.[17] The Gualtieri model allows researchers to study the nucleation and growth processes separately which can give additional information about the material as it forms.[16-17]

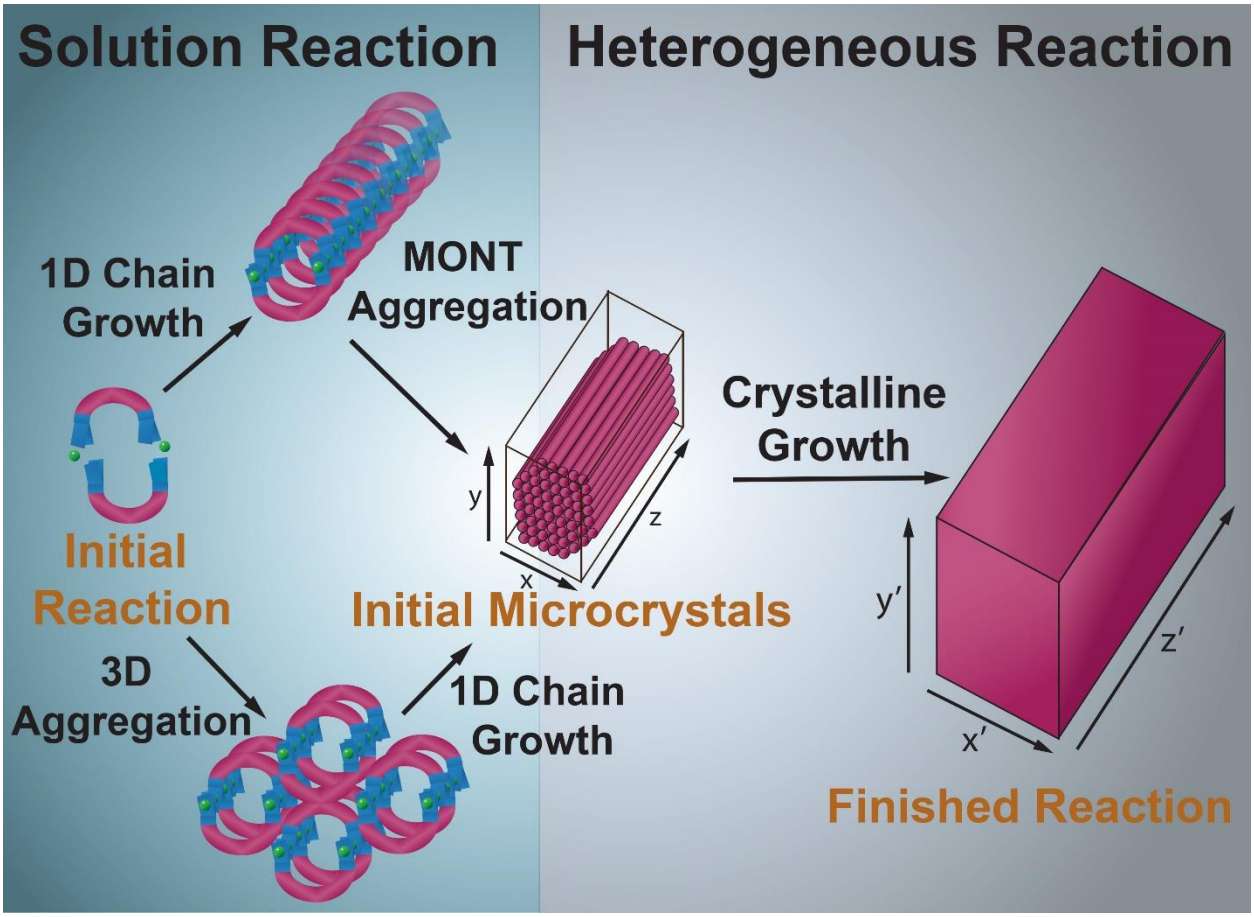

Figure 2.3. Cartoon depicting the two hypothesized mechanisms of MONT formation in solution. Small-angle X-ray scattering allows for the determination of this growth mechanism.

Analyses of the scattering profiles of the MONTs as they formed revealed the initial formation of isotropic porous structures that grow into anisotropic structures in a preferred orientation as the reaction proceeds to completion. It was observed that the rate of nucleation increases rapidly for the first 100-150 minutes of the reaction, then decreases with time. At this same point, the growth rate increases rapidly and achieves a steady state, then decreases toward zero as nucleation sites are exhausted. Kinetic analysis of the data indicated that MONT formation was autocatalytic after formation of initial microcrystals.[16]

A critical aspect of the Gualtieri model is that it incorporates a variable of dimensionality, *n*, in which $n = 1$ indicates 1D rods, $n = 2$ indicates 2D sheets, and $n = 3$ indicates an isotropic 3D material. For this study the kinetics and growth fit best when the dimensionality variable was set to $n = 1$. Because not all MONT structures in the literature are independent tubes and are more structurally similar to 2D MOFs with 1D nanotubular pores, this variable of dimensionality could prove to be a critical factor for providing a structural definition of MONTs.

A complementary SEM study was carried out to study the morphology of the MONTs as they grow through the course of the reaction. SEM images obtained at 30 s into the reaction showed inhomogeneous solids with broad size distribution (Fig. 2.4.a).[16] Notably, no rod-like structures were observed this early in the reaction. Between 15 and 120 minutes into the reaction rod-like structures with small nanobud-type structures at the surface were observed (Fig. 2.4.b), and as time progressed, thickening of the nanorods could be seen as the number of these nanobuds diminished. By 320 min the nanobuds

were absent in the micrographs and nanorods with smooth surfaces remained (Fig. 2.4.c). It is likely that these smaller structures are heterogeneous nucleation sites that adhered to the existing nanorod structures via π-π stacking in the nanotube growth phase of the reaction.

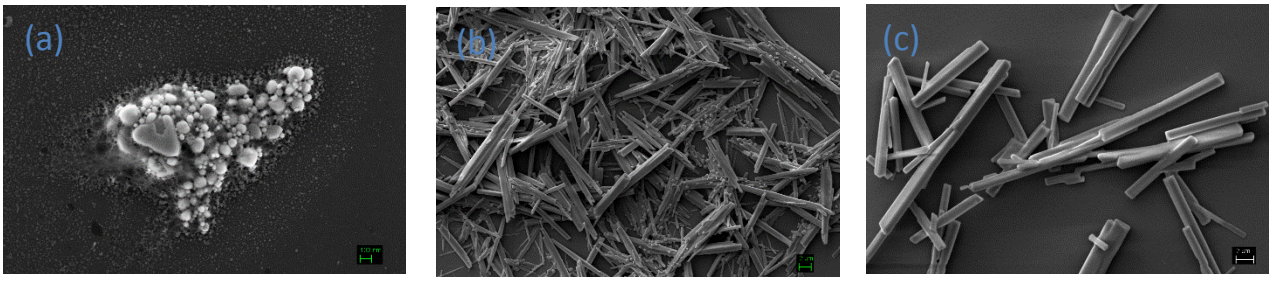

Figure 2.4. Representative SEM images of $[Ag_2(1)(NO_3)_2]$·NMP nanotubes captured after (a) 30 sec, (b) 60 min, AND (c) 320 min of reaction time. The scale bar in Figure 2.4.a represents 100 nm and in Figures 2.4.b-c represents 2 μm.[16]

Conclusions

The results outlined in detail in the manuscript published in *Crys. Growth Des.* showed that the formation of these MONTs can be drescribed as the generation of an initial isotropic porous structure immediately after mixing the metal and ligand, which then form aggregates that grow into nanorods in a preferred orientation. While this study only examined one example of a two-column pillared MONT, understanding the nucleation and growth mechanisms will be valuable for guiding further syntheses. Additionally, expanding this study to previously reported structures both from the Jenkins group and

others will allow us to evaluate generalizability of this approach for MONT characterization.

SAXS can also be employed to study MONTs when X-ray crystallographic characterization is not possible. Indeed, the overarching goal of MONT chemists is to prepare *discrete* MONTs, or MONTs that are not packed into a crystalline structure. SAXS can provide information about the diameter of rod-like structures at the sub-nanometer level; successful dispersion of MONTs will result in structures that could be as low as a dozen or less nanotubes aggregated in solution and from the diameter of the rods we will be able to extrapolate the degree of aggregation. *In situ* methods to reduce crystallite size, like addition of surfactants and templating agents that have been demonstrated to reduce crystallite size for the preparation of nanosized MOFs,[18] will be investigated in future studies by the Jenkins and Dadmun groups, and SAXS will form the primary characterization method to understand structure and size distribution.

Experimental

MONT samples were prepared according to previously published procedures developed by Dr. Christopher Murdock.[12] All other reagents were purchased from commercial vendors and used without purification.

Transmission Electron Microscopy. The dispersity of MONT samples was investigated on a Ziess Libra 200 HT FE MC at 200 kV. Around 5 mg of MONT sample

was dispersed in 0.5 mL methanol, sonicated for 5 seconds to form a suspension, then a small aliquot was pipetted onto a graphite TEM grid and left to dry overnight. For samples stained with uranyl nitrate, around 0.5 mg $UO_2(NO_3)_2$ was dissolved in 0.5 mL methanol. The MONT sample was dispersed in solution and sonicated for 5 seconds, and left to set overnight. Prior to loading the sample, the sample was sonicated for another 5 seconds, pipetted onto the TEM grid, and left to dry overnight prior to analysis.

Synthesis of 4,4′-(1,4-(xylene)diyl)bis(1,2,4-triazole). The compounds 1,2,4-triazole-1-propanenitrile, 4,4'-[1,4-(xylene)diyl]bis-(1-(2-cyanoethyl)-1,2,4-triazolium) dibromide, and 4,4′-(1,4-(xylene)diyl)bis(1,2,4-triazole) (**L**) were prepared as described previously.[12, 19]

Synthesis of silver-bis(1,2,4-triazole) nanotubes for SAXS. The silver-bis(triazole) nanotubes formation was carried out following previously reported conditions.[12] Five equivalents of $AgNO_3$ and two equivalents of the ligand (**L**) was separately dissolved in water and N-methyl-2-pyrrolidone (NMP) respectively and heated for 15 minutes until dissolved. Mixing of the two solutions leads to the formation of a white suspension that was then heated at 85 °C to form $[Ag_2(\mathbf{L})(NO_3)_2]\cdot$NMP over 3 h.

Small angle X-ray experiment. X-ray scattering measurements were performed using a high flux small angle X-ray scattering instrument (SAXSess mc^2, Antom Paar, Austria) equipped with Kratky block-collimation system and a sealed-tube Cu K_α X-ray

generator with the wavelength, λ=0.154 nm operating at tension = 40 kV and tube current = 50 mA.

Time-resolved *ex-situ* small-angle X-ray scattering measurements were performed at room temperature in transmission geometry on a series of quartz capillaries filled with the MONT solution obtained as a function of the reaction time. The reaction time is defined as the time between the mixing of the reactants to the time when the aliquots is drawn out from the reaction mixture. The MONT synthesis was carried out in a glass vial placed in a heating block at 85 °C. The acquisition time for a spectrum was approximately 15 minutes. The scattered X-ray intensities were detected by a 2D charge couple detector with a spatial resolution of 24×24μm^2 per pixel at a sample-to-detector distance of 30.9 cm.

Finally, the scattering intensities measured as a function of half the scattering angle, θ, were first corrected for the absorption of the X-rays by the sample followed by further correction for the scattering of the empty cell and transformed to a plot of scattering intensity vs. momentum transfer vector, Q ($Q = 4\pi\, sin\theta/\lambda$) using the Anton Paar SAXSquant package. The corrected data were normalized with respect to the scattering of a water sample that is measured at exactly the same conditions as the MONT samples.

Scanning electron microscopy. The morphology of the MONTs as a function of reaction time was also observed by Zeiss Dual Beam FIB/SEM instrument operated at 5 kV. The samples were prepared by placing a drop of MONT solution on a cleaned silicon oxide wafer followed by drying at room temperature and in a vacuum oven at 30 °C for

approximately 12 hours. Gold was sputtered over the samples to reduce charging and thereby improving the image quality. All the images were collected by scanning the samples at a scanning speed of 3 frames a second and averaging over 48 frames.

References

1. Iijima, S., Helical microtubules of graphitic carbon. *Nature* **1991,** *354*, 56-58.
2. Iijima, S.; Ichihashi, T., Single-shell carbon nanotubes of 1-nm diameter. *Nature* **1993,** *363*, 603-605.
3. Odom, T. W.; Huang, J.-L.; Kim, P.; Lieber, C. M., Atomic structure and electronic properties of single-walled carbon nanotubes. *Nature* **1998,** *391*, 62-64.
4. (a) Islam, A. E.; Rogers, J. A.; Alam, M. A., Recent Progress in Obtaining Semiconducting Single-Walled Carbon Nanotubes for Transistor Applications. *Adv. Mater.* **2015,** *27*, 7908-7937; (b) Itkis, M. E.; Pekker, A.; Tian, X.; Bekyarova, E.; Haddon, R. C., Networks of Semiconducting SWNTs: Contribution of Midgap Electronic States to the Electrical Transport. *Acc. Chem. Res.***2015,** *48*, 2270-2279; (c) Kharlamova, M. V., Advances in tailoring the electronic properties of single-walled carbon nanotubes. *Prog. Mater. Sci.* **2016,** *77*, 125-211.
5. (a) Ameen, A. A.; Giordano, A. N.; Alston, J. R.; Forney, M. W.; Herring, N. P.; Kobayashi, S.; Ridlen, S. G.; Subaran, S. S.; Younts, T. J.; Poler, J. C., Aggregation kinetics of single-walled carbon nanotubes investigated using mechanically wrapped multinuclear complexes: probing the tube-tube repulsive barrier. *Phys. Chem. Chem. Phys.* **2014,** *16*, 5855-5865; (b) Azoz, S.; Gilbertson, L. M.; Hashmi, S. M.; Han, P.; Sterbinsky, G. E.; Kanaan, S. A.; Zimmerman, J. B.; Pfefferle, L. D., Enhanced dispersion and electronic performance of single-walled carbon nanotube thin films without surfactant: A comprehensive study of various treatment processes. *Carbon* **2015,** *93*, 1008-1020; (c) Forney, M. W.; Poler, J. C., Significantly Enhanced Single-Walled Carbon Nanotube Dispersion Stability in Mixed Solvent Systems. *J. Phys. Chem. C* **2011,** *115*, 10531-10536; (d) Koh, B.; Cheng, W., The Impact of Sonication on the Surface Quality of Single-Walled Carbon Nanotubes. *J. Pharm. Sci.* **2015,** *104*, 2594-2599.
6. (a) Azoz, S.; Exarhos, A. L.; Marquez, A.; Gilbertson, L. M.; Nejati, S.; Cha, J. J.; Zimmerman, J. B.; Kikkawa, J. M.; Pfefferle, L. D., Highly Conductive Single-Walled Carbon Nanotube Thin Film Preparation by Direct Alignment on Substrates from Water Dispersions. *Langmuir* **2015,** *31*, 1155-1163; (b) Devre, R. D.; Budhlall, B. M.; Barry, C. F., Enhancing the Colloidal Stability and Electrical Conductivity of Single-Walled Carbon Nanotubes Dispersed in Water. *Macromol. Chem. Phys.* **2016,** *217*, 683-700.
7. (a) Chen, G.; Davis, R. C.; Futaba, D. N.; Sakurai, S.; Kobashi, K.; Yumura, M.; Hata, K., A sweet spot for highly efficient growth of vertically aligned single-walled carbon nanotube forests enabling their unique structures and properties. *Nanoscale* **2016,** *8*, 162-171; (b) Chen, G.; Futaba, D. N.; Kimura, H.; Sakurai, S.; Yumura, M.; Hata, K., Absence of an Ideal Single-Walled Carbon Nanotube Forest Structure for Thermal and Electrical Conductivities. *ACS Nano* **2013,** *7*, 10218-10224.
8. Thanasekaran, P.; Luo, T.-T.; Lee, C.-H.; Lu, K.-L., A journey in search of single-walled metal-organic nanotubes. *J. Mater. Chem.***2011,** *21*, 13140-13149.
9. (a) Devan, R. S.; Patil, R. A.; Lin, J.-H.; Ma, Y.-R., One-Dimensional Metal-Oxide Nanostructures: Recent Developments in Synthesis, Characterization, and

Applications. *Adv. Funct. Mater.* **2012,** *22*, 3326-3370; (b) Golberg, D.; Bando, Y.; Tang, C. C.; Zhi, C. Y., Boron Nitride Nanotubes. *Adv. Mater.* **2007,** *19*, 2413-2432; (c) Lee, K.; Mazare, A.; Schmuki, P., One-Dimensional Titanium Dioxide Nanomaterials: Nanotubes. *Chem. Rev.* **2014,** *114*, 9385-9454; (d) Li, Y.; Yang, X.-Y.; Feng, Y.; Yuan, Z.-Y.; Su, B.-L., One-Dimensional Metal Oxide Nanotubes, Nanowires, Nanoribbons, and Nanorods: Synthesis, Characterizations, Properties and Applications. *Crit. Rev. Solid State Mater. Sci.* **2012,** *37*, 1-74; (e) Wang, J.; Lee, C. H.; Yap, Y. K., Recent advancements in boron nitride nanotubes. *Nanoscale* **2010,** *2*, 2028-2034; (f) Zhi, C.; Bando, Y.; Tang, C.; Golberg, D., Boron nitride nanotubes. *Mater. Sci. Eng. R* **2010,** *70*, 92-111.

10. Dai, F.; He, H.; Sun, D., A Metal−Organic Nanotube Exhibiting Reversible Adsorption of $(H_2O)_{12}$ Cluster. *J. Am. Chem. Soc.* **2008,** *130*, 14064-14065.
11. (a) Fukino, T.; Joo, H.; Hisada, Y.; Obana, M.; Yamagishi, H.; Hikima, T.; Takata, M.; Fujita, N.; Aida, T., Manipulation of Discrete Nanostructures by Selective Modulation of Noncovalent Forces. *Science* **2014,** *344*, 499-504; (b) Yamagishi, H.; Fukino, T.; Hashizume, D.; Mori, T.; Inoue, Y.; Hikima, T.; Takata, M.; Aida, T., Metal–Organic Nanotube with Helical and Propeller-Chiral Motifs Composed of a C_{10}-Symmetric Double-Decker Nanoring. *J. Am. Chem. Soc.* **2015,** *137*, 7628-7631.
12. Murdock, C. R.; Jenkins, D. M., Isostructural Synthesis of Porous Metal–Organic Nanotubes. *J. Am. Chem. Soc.* **2014,** *136*, 10983-10988.
13. (a) Cenker, Ç. Ç.; Bomans, P. H. H.; Friedrich, H.; Dedeoğlu, B.; Aviyente, V.; Olsson, U.; Sommerdijk, N. A. J. M.; Bucak, S., Peptide nanotube formation: a crystal growth process. *Soft Matter* **2012,** *8*, 7463-7470; (b) Graveland-Bikker, J. F.; Fritz, G.; Glatter, O.; De Kruif, C. G., Growth and structure of α-lactalbumin nanotubes. *J. Appl. Crystallogr.* **2006,** *39*, 180-184; (c) Landau, M. V.; Vradman, L.; Wang, X.; Titelman, L., High loading TiO_2 and ZrO_2 nanocrystals ensembles inside the mesopores of SBA-15: preparation, texture and stability. *Microporous Mesoporous Mater.* **2005,** *78*, 117-129; (d) Maillet, P.; Levard, C.; Larquet, E.; Mariet, C.; Spalla, O.; Menguy, N.; Mason, A.; Doelsch, E.; Rose, J.; Thill, A., Evidence of Double-Walled Al−Ge Imogolite-Like Nanotubes. A Cryo-TEM and SAXS Investigation. *J. Am. Chem. Soc.* **2010,** *13*, 1208-1209.
14. (a) Demortière, A.; Schaller, R. D.; Li, T.; Chattopadhyay, S.; Krylova, G.; Shibata, T.; dos Santos Claro, P. C.; Rowland, C. E.; Miller, J. T.; Cook, R.; Lee, B.; Shevchenko, E. V., In Situ Optical and Structural Studies on Photoluminesence Quenching in CdSe/CdS/Au Heterostructures. *J. Am. Chem. Soc.* **2014,** *136*, 2342-2350; (b) Hubert, F.; Testard, F.; Thill, A.; Kong, Q.; Tache, O.; Spalla, O., Growth and Overgrowth of Concentrated Gold Nanorods: Time Resolved SAXS and XANES. *Cryst. Growth Des.* **2012,** *12*, 1548-1555; (c) Morita, T.; Hatakeyama, Y.; Nishikawa, K.; Tanaka, E.; Shingai, R.; Murai, H.; Nakano, H.; Hino, K., Multiple small-angle X-ray scattering analyses of the structure of gold nanorods with unique end caps. *Chem. Phys.* **2009,** *364*, 14-18; (d) Tsao, C.-S.; Chuang, C.-M.; Chen, C.-Y.; Huang, Y.-C.; Cha, H.-C.; Hsu, F.-H.; Chen, C.-Y.; Tu, Y.-C.; Su, W.-F., Reaction Kinetics and Formation Mechanism of TiO2 Nanorods in Solution: An Insight into Oriented Attachment. *J. Phys. Chem. C* **2014,** *118*, 26332-26340.

15. (a) Holt, A. P.; Griffin, P. J.; Bocharova, V.; Agapov, A. L.; Imel, A. E.; Dadmun, M. D.; Sangoro, J. R.; Sokolov, A. P., Dynamics at the Polymer/Nanoparticle Interface in Poly(2-vinylpyridine)/Silica Nanocomposites. *Macromolecules* **2014,** *47* (5), 1837-1843; (b) Imel, A. E.; Dadmun, M. D., The impact of fullerenes on the ordering of polyacrylonitrile during nanocomposites formation. *Polymer* **2015,** *75*, 134-140; (c) Jin, N.; Zhang, H.; Jin, S.; Dadmun, M. D.; Zhao, B., Shifting Sol–Gel Phase Diagram of a Doubly Thermosensitive Hydrophilic Diblock Copolymer Poly(methoxytri(ethylene glycol) acrylate-co-acrylic acid)-b-poly(ethoxydi(ethylene glycol) acrylate-co-acrylic acid) in Aqueous Solution. *Macromolecules* **2012,** *45*, 4790-4800.
16. Etampawala, T.; Mull, D. L.; Keum, J. K.; Jenkins, D. M.; Dadmun, M., Insights into the Morphology and Kinetics of Growth of Silver Metal–Organic Nanotubes. *Cryst. Growth Des.* **2016,** *16*, 1395-1403.
17. Gualtieri, F. A., Synthesis of sodium zeolites from a natural halloysite. *Phys. Chem. Miner. 28*, 719-728.
18. (a) Seoane, B.; Dikhtiarenko, A.; Mayoral, A.; Tellez, C.; Coronas, J.; Kapteijn, F.; Gascon, J., Metal organic framework synthesis in the presence of surfactants: towards hierarchical MOFs? *CrystEngComm* **2015,** *17*, 1693-1700; (b) Taylor, K. M. L.; Rieter, W. J.; Lin, W., Manganese-Based Nanoscale Metal−Organic Frameworks for Magnetic Resonance Imaging. *J. Am. Chem. Soc.* **2008,** *130*, 14358-14359.
19. Murdock, C. R.; McNutt, N. W.; Keffer, D. J.; Jenkins, D. M., Rotating Phenyl Rings as a Guest-Dependent Switch in Two-Dimensional Metal–Organic Frameworks. *J. Am. Chemi. Soc.* **2014,** *136*, 671-678.

CHAPTER 3
DESIGNING LIGANDS TO FACILITATE THE SYNTHESIS OF DISCRETE METAL-ORGANIC NANOTUBES

Part of the work outlined in this chapter was carried out with help from a former undergraduate student in the Jenkins group, Khanh Pham.

Abstract

Metal-organic nanotubes (MONTs) are low-dimensional variants of metal-organic frameworks (MOFs) in which independent, 1D tubes pack into 3D crystalline lattices. Their crystal packing makes them indistinguishable from MOFs, effectively limiting their development for applications that require highly anisotropic, 1D materials. This chapter details efforts to post-synthetically disperse packed MONTs to individual tubes, and devise strategies to reduce aggregation and crystal packing to simplify the design of low-dimensional materials.

Introduction

The preparation of discrete metal-organic nanotubes (MONTs) is a challenge currently pursued by a handful of chemists and materials scientists across the globe. These materials are the 1D variant of metal-organic frameworks (MOFs), and although many of the published structures reveal independent, 1D tubes,[1] all but two examples published by Aida's group[2] are packed in 3D, effectively limiting their potential as highly anisotropic materials. Two challenges face chemists and engineers who pursue discrete MONTs: post-synthetic reduction of the MONT crystallite size to nanotube bundles comprised of tens of nanotubes could cause rapid sample degradation as most coordination materials are held together by relatively weak bonds, and characterization

of low dimensional materials requires instrumentation that only gives structural and morphological details without information regarding molecular connectivity.

Typically, low-dimensional materials are characterized by electron microscopic methods that are suitable for their size regime. Scanning electron microscopy (SEM) is best suited for bulk materials and low-dimensional materials at the sub-micron scale whereas transmission electron microscopy (TEM) can provide much higher resolution images at the sub-nanometer scale with detailed 2D and 3D morphological and structural information in the micrographs. While TEM has been employed to study inorganic materials, metal-organic frameworks, and biological samples, in some cases the high energy electron beam can cause sample degradation before the sample can be imaged.[3] Indeed, stains like uranyl acetate and deposition of gold is necessary to preserve the sample and increase conduction of electrons to obtain an image,[3] but this does not work for every sample, limiting its widespread use as a routine characterization tool for many organic materials.

To mitigate this issue, it is necessary to employ alternative routes that can yield detailed structural information about the material of interest. As discussed in the previous chapter, small-angle X-ray scattering (SAXS) offers a versatile route to characterize discrete nanotubes or nanotube bundles as they form.[4] SAXS has been used to study the growth mechanism and structural features of transition metal chalcogenide nanorods, particularly length and diameter.[5] Employing SAXS to understand the growth mechanism will guide researchers to devise methods to inhibit nanotube aggregation to form bulk crystalline material during the course of the reaction. Because SAXS can provide

structural information, we envisage that it can also serve to characterize the size and length of the individual nanotubes or nanotube bundles through the course of the reaction.

Results and Discussion

Prior to our shifting focus to SAXS studies of MONTs, our rationale was to prepare isostructural nanotubes with increased pore diameter that can be readily visualized with TEM. By preparing larger, semi-rigid ligands that can adopt a *syn* conformation in solution, we can follow the principles of isoreticularity established by Yaghi[6] to synthesize materials that have the same metal and bonding but increased dimensions. The route to prepare the ligands that were employed to synthesize the first isostructural series of MONTs[1f] can be seen in Scheme 3.1.A. By applying of the method pioneered by Horváth,[7] our group was able to synthesize pure, semi-rigid ditriazole ligands by reacting 1,4-bis(bromomethyl)benzene (**1**) with 3-(1H-1,2,4-triazol-1-yl)propanenitrile (**2**) in refluxing acetonitrile to prepare the dicationic intermediate **3**, which can then be deprotected with potassium hydroxide in water to form the *para*-xylyl ligand **4**. This route was generalizable in that aromatic moieties of varying sizes could be incorporated into the backbone of the ligand.[1f] This route, however, limits the ability to prepare extended linkers in which both the height and width of the nanotube can be tuned separately. Addition of an aromatic moiety between the methylene bridge and the coordinating 1,2,4-triazole units appeared to be the most direct method to prepare height-and-width adjustable ligands, and it was anticipated that coupling between aryl boronic acid pinacol esters and benzylic bromides, as outlined in Scheme 3.1.B, would allow us to synthesize the desired targets.

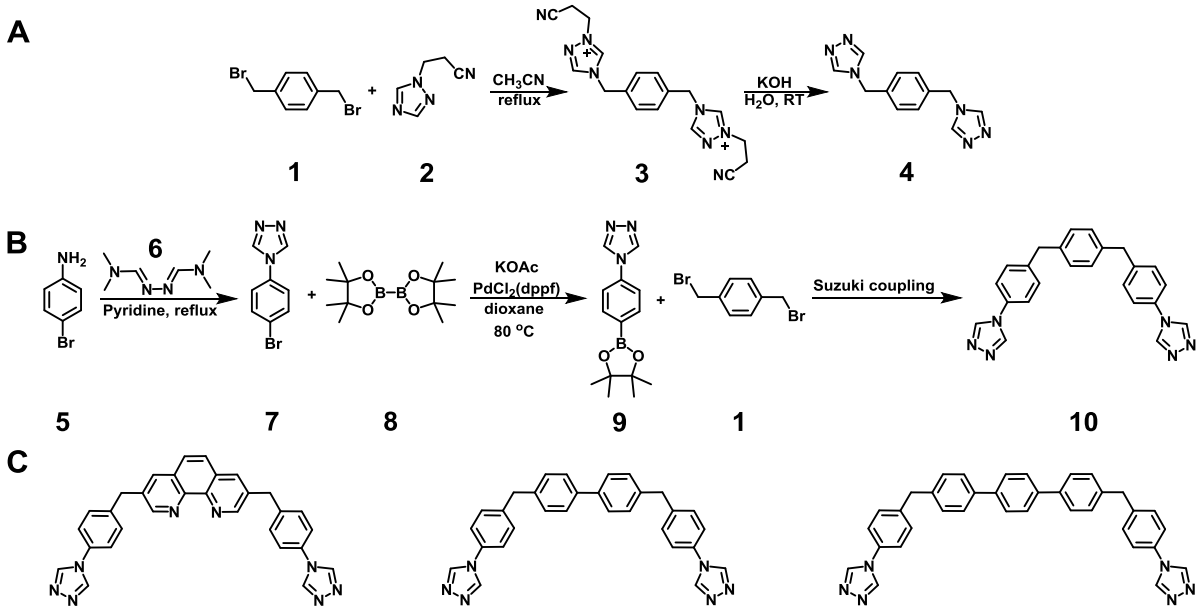

Scheme 3.1. A) Original method adapted from Horváth's procedure to prepare semi-rigid di-triazole linkers. B) Original route pursued to prepare height- and width-adjustable linkers. C) Example target ligands.

Target synthons for extended linkers are shown in Scheme 3.1.B. The starting material 4-bromoaniline (**5**) was refluxed in pyridine with (E)-N'-((E)-(dimethylamino)methylene)-N,N-dimethylformohydrazonamide (**6**) to obtain 4-(4-bromophenyl)-4H-1,2,4-triazole (**7**). The product was subjected to Miyaura Borylation conditions in which **7** was coupled to bis(pinacolato)diboron (**8**), which yielded 4-(4-(4,4,5,5-tetramethyl-1,3,2-dioxaborolan-2-yl)phenyl)-4H-1,2,4-triazole (**9**). After diluting the reaction mixture with EtOAc, filtering over Celite, and removing solvent *in vacuo*, the crude product was purified by flash chromatography in 2-5% MeOH in CH_2Cl_2. With each isolated solid, a consistent impurity was observed that exhibited a large singlet below 1.5 ppm in the ^{1}H-NMR spectrum. It was speculated to be a byproduct of bis(pinacolato)diboron, though no mass spectrometry or other spectroscopic evidence

found to support this. The best separation was achieved following elution in 5% MeOH in CH_2Cl_2, and molecule **9** could be obtained as a pure, tan solid following recrystallization from EtOAc. One particularly successful recrystallization resulted in large block crystals that were suitable for single crystal X-ray diffraction (SCXRD), and the crystal structure is shown in Figure 3.1.

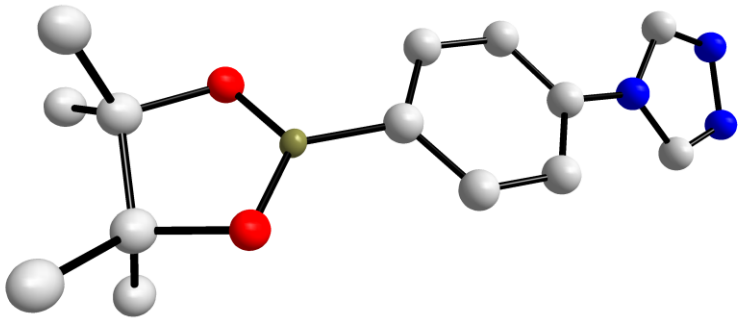

Figure 3.1. Crystal structure of isolated and purified boronic acid pinacol ester. Gray, blue, red, and brown ellipsoids represent C, N, O, and B respectively. All hydrogens were omitted for clarity.

Initial coupling test reactions were carried out under standard Suzuki Coupling conditions to prepare molecule **10** as Wu and coworkers,[8] Domínguez and coworkers,[9] Taylor and coworkers,[10] and Bandgar and coworkers[11] found success by coupling aromatic boronic acids or their pinacol esters with functionalized benzylic halides under similar conditions. For our system, no coupling was observed under any conditions. It is likely that the palladium preferred coordination from the triazole moieties and prevented oxidative insertion into the C-Br bond into initiate the catalytic cycle.

To mitigate this, it was thought that it might be more energetically favorably to employ a di-boronic acid or di-boronic acid pinacol ester as coupling synthons as the reagents were readily available within the laboratory. Forming the 1,2,4-triazole at the end of the sequence (Scheme 3.2) would circumvent this difficulty facing the coupling reaction. Some initial conditions were tested using standard pre-catalyst, ligand, base, and solvent combinations with little success. The preliminary conditions investigated are listed in Table 3.1, and unsurprisingly no coupling product was detected by DART mass spec. The next step was to evaluate additional ligands for catalysis, but the focus of the project shift from the preparation of tunable ligands to preparing ligands that inhibit nanotube aggregation as they form.

We chose to investigate the role of functional groups as a means to reduce the crystallite size of our MONTs as they form because their aggregation is driven by π-π stacking, and bulky functional groups on the aromatic backbone are an obvious way to disrupt these intermolecular interactions. The most direct route to prepare a large ligand library with bulky substituents was to functionalizing aromatic phenols with alkyl groups of increasing length and steric bulk (Figure 3.2.A and 3.2.B). A trimethyl-silyl (TMS) functionalized ligand was selected as a route to prepare a library of ether-functionalized ditriazole ligands through a divergent synthetic approach, as well as for its large steric bulk. Ligands based on solely alkyl-functionalized benzene rings were also selected based on their ready availability (Figure 3.2.B). Though our previous SAXS studies were on MONTs prepared with the *para*-xylyl ditriazole ligand, we decided to focus on the *meta*-xylyl isomer because it will be isostructural to one previously prepared MONT, and

because its symmetry will facilitate characterization by single crystal X-ray diffraction if single crystals formed.

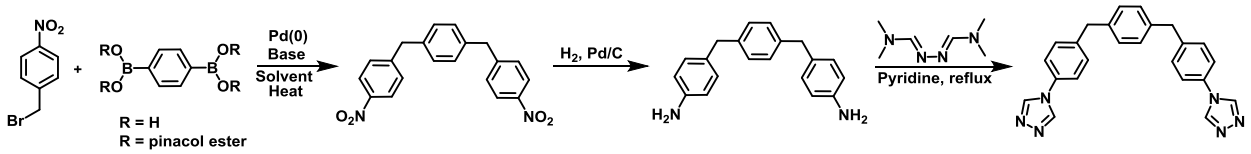

Scheme 3.2. Modified route to height and width-adjustable ligands.

Table 3.1. Representative conditions employed for benzylic coupling reactions.

R	Base	Catalyst/Ligand	Solvent/s	Temp./ °C
H	K_2CO_3	$Pd(dba)_3$	Anhydrous dioxane	Reflux
H	K_2CO_3	$Pd(dba)_3$	DMF	100 °C
H	K_2CO_3	$Pd(dba)_3$	THF	Reflux
H	K_2CO_3	$Pd(PPh_3)_4$	DMF	Reflux
Pinacol ester	K_2CO_3	$Pd(PPh_3)_4$	Dioxane	100 °C
Pinacol ester	K_2CO_3	$PdCl_2(dppf)$	Dioxane	80 °C
Pinacol ester	K_2CO_3	$Pd(PPh_3)_4$	DMF (anhydrous)	Reflux
Pinacol ester	K_2CO_3	$Pd(PPh_3)_4$	DMF	100 °C
Pinacol ester	Na_2CO_3	$Pd(PPh_3)_4$	DMF/H_2O	100 °C

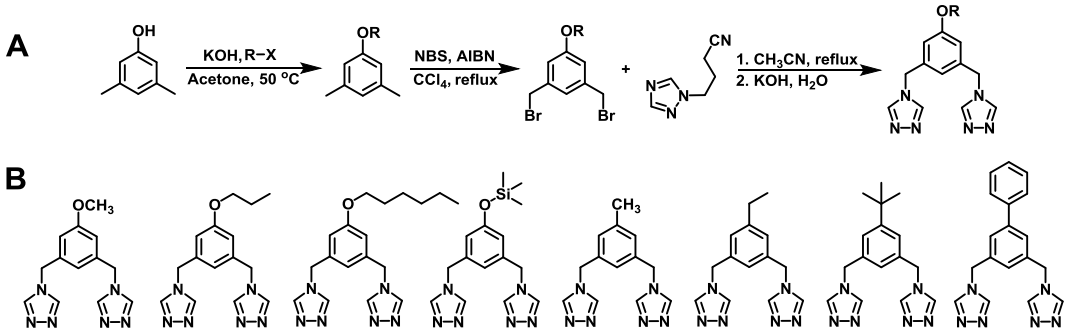

Scheme 3.3. A) General scheme to prepare alkyl-ether-functionalized ligands. B) Functionalized ligand targets to block MONT aggregation as they form.

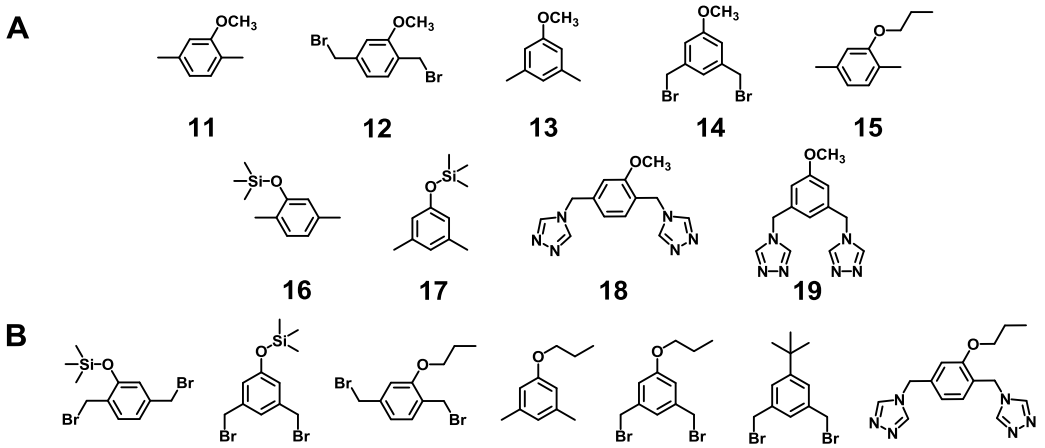

Figure 3.2. A) Molecules synthesized and fully characterized by NMR. B) Molecules that were never fully characterized by NMR due to failure to purify.

Synthesis of the ether-functionalized ligands began with the initial alkylation step that resulted in formation of colorless liquids that were purified by vacuum distillation. The bromination step was carried out with *N*-bromosuccinimide (NBS), a well-known radical bromination reagent, in refluxing carbon tetrachloride. This reaction resulted in the formation of numerous side products for each molecule synthesized, and for each case,

it was not possible to control side-product formation by adjusting temperature or radical initiator. Purification of the brominated products proved exceedingly difficult.

Several solvent systems and polarities were investigated for purifying molecules **12** and **14**. The *para* isomer **12** and those listed in Figure 3.3.B were the initial targets synthesized prior to shifting focus to exclusively *meta* isomers. For each molecule, the product spot was the top spot on the TLC plate at the end of the reaction, indicating that the spots below were species brominated to a greater degree. The *meta* isomer **14**, and the three listed in Figure 3.3.B., resulted in a distribution of mono, di-, tri-, and tetra-brominated species, with the di-brominated being the favored product; there was no residual mono-brominated product for the *para* isomers. Isolation of each brominated molecule in Figure 3.3.A and B consistently yielded either minor or major impurities in the ^{1}H and ^{13}C NMR spectra. The peaks were consistent with an asymmetric bromination product but no mass spectrometry data could be obtained to verify the molecular weight.

Additional purification methods like recrystallization, solid-phase extraction, and vacuum sublimation were employed as a means to clean up the mixture, but unfortunately all attempts were unsuccessful. The similar polarities and relatively minor differences in mass percentage between the di-brominated, tri- and tetra-brominated species made separation by sublimation quite challenging. One successful purification method to prepare molecule **14** involved concentrating the crude product, filtering over a silica gel plug by eluting in a 5% ethyl acetate in hexanes solution, and concentrating the filtrate to obtain a yellow oil composed of the mono- and di-brominated intermediates. The di-brominated intermediate crashed out as colorless, needle crystals over 3 d and was

collected in 28% yield after washing with hexanes. This method was not consistently reproducible for preparing pure **14**. The difficulty of purification warranted examining other routes with easier purification regimes to prepare the brominated intermediates.

The pure product was then used to prepare the final ligand after subjecting to the same conditions as those outlined in Scheme 3.1.A. The product was soluble in water and to a lesser degree ethanol. The product can be extracted from water with chloroform or a 1:1 chloroform:ethanol combination, or the deprotection step can be carried out in refluxing ethanol. From the latter route, the byproduct, postassium bromide, can be filtered off as the reaction cools. Previous purification involved recrystallization from ethanol, but future attempts to follow this procedure should employ Soxhlet extraction from dichloromethane as shown previously by Jenkins and coworkers.[1f] A few attempts were made to prepare isoreticular MONTs with the methoxy-functionalized ligand but within a few days the reaction mixture turned brown-black. Though the ^{1}H- and ^{13}C-NMR spectra showed no additional peaks, it is likely that residual salts still present in the sample reacted with the metal salt starting material to cause it to reduce.

In addition to studies that focused on the synthesis of extended and functionalized ligands, additional work was carried out to employ tetrazole-based ligands. Tetrazoles are five membered rings that are composed of four nitrogen atoms, and can be deprotonated in solution to form an anionic, aromatic coordinating unit. Reacting these type of anionic ligands with metal salts to form MONTs could prove beneficial as the vast majority of MOF structures have been prepared with anionic linkers, and a handful of MOF structures that utilize tetrazole-based ligands have been reported. Indeed,

employing semi-rigid, ditetrazole linkers could form MONTs that are isostructural to the nanotubes our group previously reported, but because of the dianionic nature of the ligands after deprotonation, the ligands would balance the charge from divalent cations, like Cu^{2+}, Ni^{2+}, and Pd^{2+}, limiting the need for counter anions to charge balance the framework. Charge balancing would be beneficial because it would increase available pore space within the nanotubes and most likely decrease the reliance on bridging halides and weak electron donors to hold the MONT structure together. This route could prove to be useful for preparing nanometer-scale crystallites of MONTs.

The scheme to prepare the ditetrazole linker is shown in Scheme 3.4. Refluxing 1,4-bis(chloromethyl)benzene (**20**) with sodium cyanide in acetonitrile overnight forms the dinitrile intermediate 2,2'-(1,4-phenylene)diacetonitrile (**21**). The crude product could be immediately used in the next step in which the **21** was refluxed for 3 d in toluene with sodium azide and triethylamine hydrochloride to form the final tetrazole product, 1,4-bis((2H-tetrazol-5-yl)methyl)benzene (**22**). After cooling to room temperature and concentrating the toluene, the product could be extracted using 1 M NaOH. Any residual solid was filtered off with a frit and the pure product was isolated after addition of a large excess of 6 M aqueous HCl to reach a pH = 1. Filtration yielded the white powder, which after rinsing with water and diethyl ether, then drying under high vacuum overnight, was confirmed to be the pure tetrazole linker.

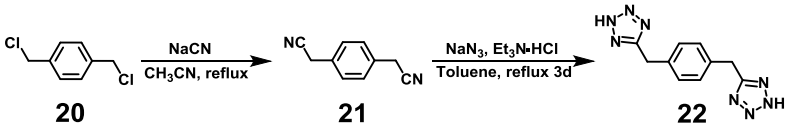

20 **21** **22**

Scheme 3.4. Direct route to prepare semigrid ditetrazole ligand for incorporation into new metal-organic nanotube structures.

Thousands of reaction conditions were screened with the tetrazole linker. Initial trials carried out in amide solvent/water combinations, more specifically *N,N*-dimethylformamide (DMF), *N,N*-diethylformamide (DEF), *N,N*-dimethylacetamide (DMA), and *N*-methyl-2-pyrrolidone (NMP), resulted in the formation of gels almost instantly after mixing the ligand and metal solutions together. Small bubbles could be observed evolving from the gel network, most likely H_2 gas due to the presence of acidic protons on the tetrazole and the presence of water. Initially gel formation was initially thought to be a result of solvent polymerization until it was observed in an ethanol/water combination. It is possible that the reaction mixture could be undergoing a sol-gel type reaction to form a metal-oxide material. This product from this undesired reaction was not investigated but instead efforts were devoted to mitigate gel formation.

Tetrazole protons are acidic and are therefore sensitive to pH adjustments. Previously reported MOF structures that were synthesized with aromatic tetrazole ligands have employed buffers or added aliquots of acid to control the pH and slow the crystal nucleation and growth processes. Addition of small aliquots of concentrated acids like hydrochloric acid, sulfuric acid, nitric acid, and acetic acid to the reaction conditions were investigated to determine if acid identity and concentration could mitigate gel formation or affect how a potential framework crystallizes. Unfortunately, this route only exacerbated the gel formation, indicating that a higher pH is better suited to prepare crystalline material with this ligand.

Buffered solutions between pH = 2 – 8 were prepared following standard procedures and used in MONT test reactions by first dissolving the metal salt precursor

in the buffered solution, then reacting with the tetrazole ligand dissolved in an organic solvent that is miscible with water. One successful test reaction yielded a vivid blue microcrystalline sample after dissolving the tetrazole ligand in DMA and copper (II) sulfate pentahydrate in an aqueous solution buffered to a pH of 5.38 and heating for two weeks. The powder X-ray diffraction (PXRD) pattern is shown in Figure 3.3.A in red. Despite attempts to reproduce the sample, all further attempts were unsuccessful.

Two more samples prepared from $CuSO_4$ yielded microcrystalline samples. The tetrazole ligand was dissolved in water following the addition of a 2:1 molar ratio of KOH to ligand to completely deprotonate the tetrazole, and the metal salt was dissolved in aqueous tris(hydroxymethyl)aminomethane/HCl buffer solution adjusted to a pH = 8. Two samples formed crystalline material under these conditions when the metal salt, $CuSO_4 \cdot 5H_2O$, and the ligand were mixed in a 2:1 and 4:1 metal-to-ligand (M:L) ratio. The PXRD patterns are shown in Figure 3.3.B and C, respectively.

Three other microcrystalline samples were prepared with the tetrazole ligand. Reactions were carried out between $AgNO_3$ and the tetrazole ligand in combinations of DMF/H_2O, DEF/H_2O, and DMA/H_2O at a M:L ratio of 2:1 for all three. The critical step was to cool the ligand and metal solutions to around 0 °C prior to mixing as a means to inhibit the polymerization/sol-gel reaction that occurs at room temperature mixing. Mixing of the solutions at low temperatures forms an amorphous white solid, which after allowing the solutions to warm to room temperature and heating at 85 °C for 3 h, a white microcrystalline solid was obtained. The PXRD patterns for the samples prepared in DMF, DEF, and DMA are shown in Figure 3.3.D, E, and F, respectively. The most crystalline

sample was prepared in DEF (Figure 3.3.E), but these samples were not reproducible, thus limiting further studies.

The IR spectra for each of the powder crystalline samples discussed above are shown in Figure 3.4.A-F, and the colors for each sample are consistent for each sample shown in Figure 3.3.A-F. The IR spectrum of the original tetrazole linker is shown in black in Figure 3.4.G. The IR spectra show that the tetrazole is bound to the metal in each of the samples, and because each sample is crystalline and exhibit low angle peaks in the PXRD pattern, it is highly likely that a porous material has formed. The dimensionality of the structures is unknown but for samples prepared from the same metal, the samples are clearly isostructural if not identical.

As discussed in Chapter 2, we established a collaboration with the Dadmun group to employ small-angle X-ray scattering (SAXS) to study the structure, mechanisms of nucleation and growth, and the kinetics of formation of MONTs. As part of our continued work we proposed to investigate the formation of two other known MONTs and one sample prepared with the tetrazole. Prior to data collection a series of samples were prepared and heated for a pre-determined amount of time and imaged using SEM to determine the best time slices to examine with SAXS. In the process we were able to obtain images of the $CuSO_4 \cdot 5H_2O$ and the tetrazole reacted in a 2:1 metal-to-ligand ratio. Figure 3.6 shows an SEM image of a Cu sample, for which the PXRD pattern is shown in Figure 3.4.B. The micrograph showed needle structures that were bundled together, potentially indicative of π-π stacking in the structure. The length of the needles was greater than 2 μm as indicated by the scale bar in the bottom of the figure. Initial trials to run

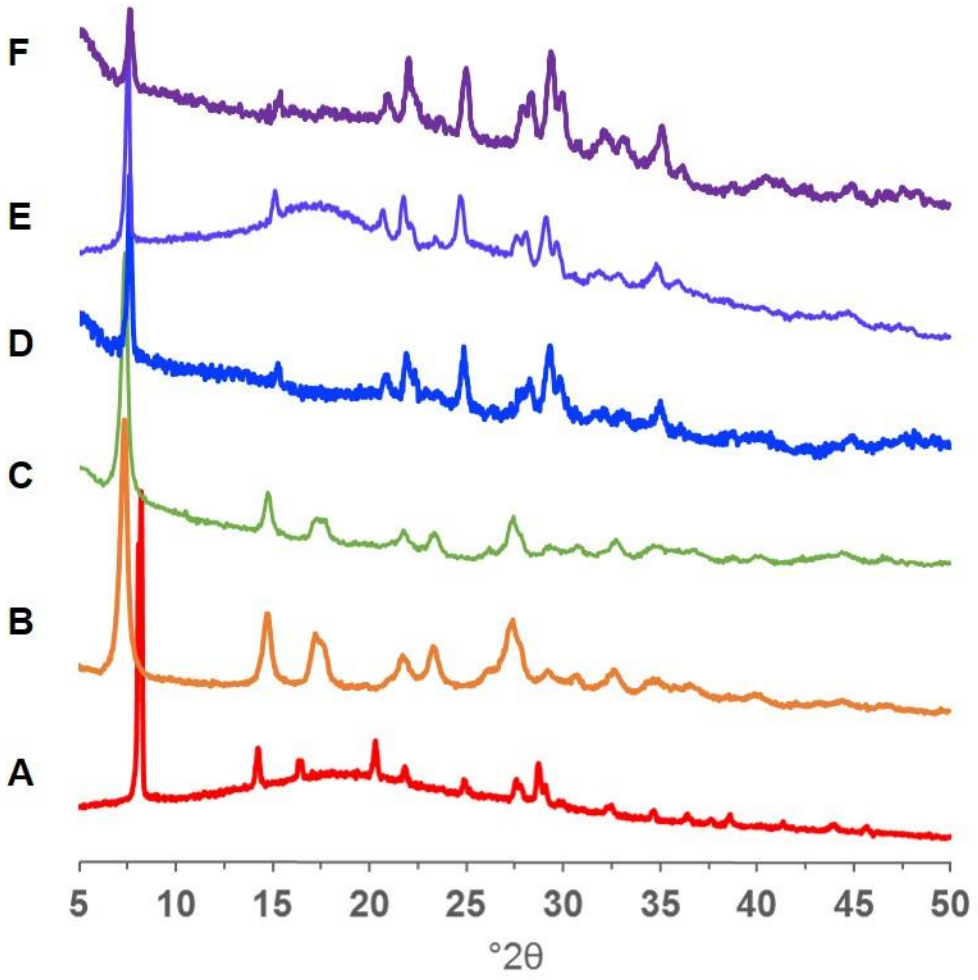

Figure 3.3. PXRD patterns of microcrystalline samples prepared from the tetrazole ligand and A) $CuSO_4 \cdot 5H_2O$ in DMA and aqueous buffer with a pH = 5.38, B) $CuSO_4 \cdot 5H_2O$ in a M:L = 2:1, KOH, and aqueous buffer with a pH = 8, C) $CuSO_4 \cdot 5H_2O$ in a M:L = 4:1, KOH, and aqueous buffer with a pH = 8, and $AgNO_3$ in a M:L = 2:1 in D) DMF, E) DEF) AND F) DMA.

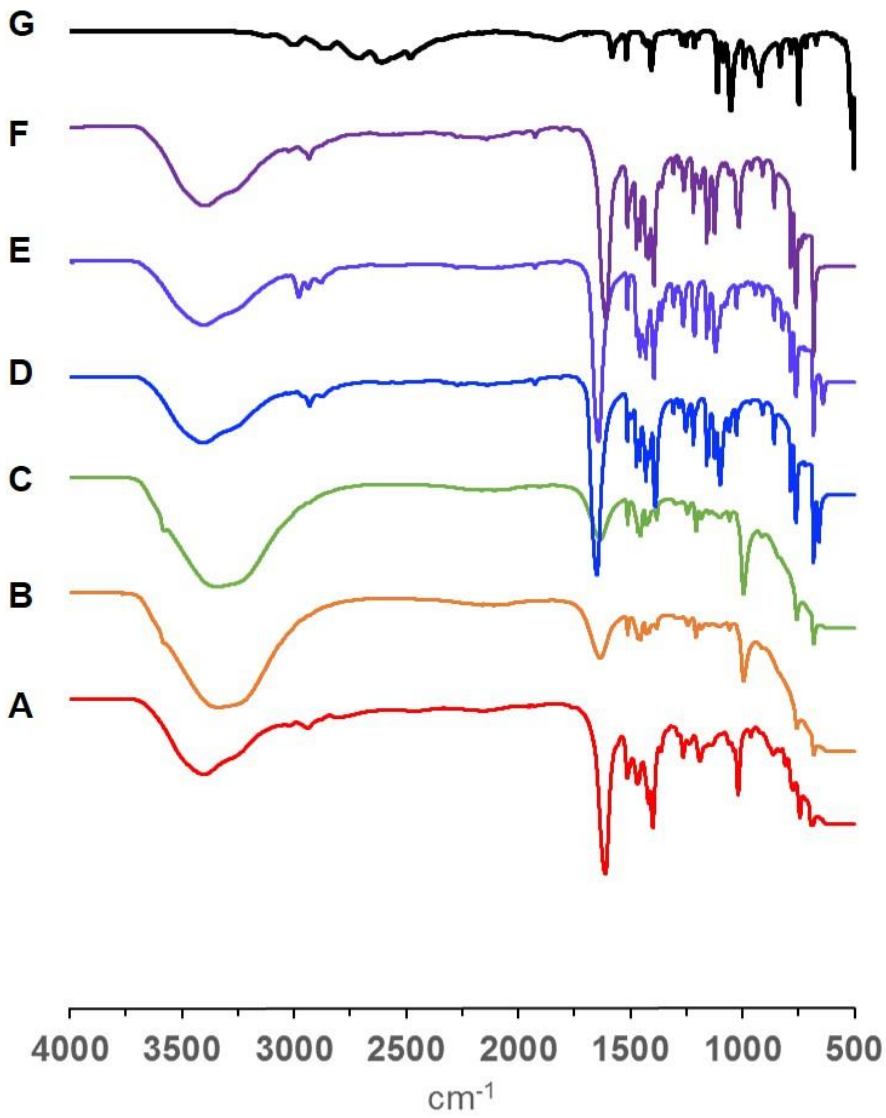

Figure 3.4. IR spectra of microcrystalline samples prepared from the tetrazole ligand and A) $CuSO_4 \cdot 5H_2O$ in DMA and aqueous buffer with a pH = 5.38, B) $CuSO_4 \cdot 5H_2O$ in a M:L = 2:1, KOH, and aqueous buffer with a pH = 8, C) $CuSO_4 \cdot 5H_2O$ in a M:L = 4:1, KOH, and aqueous buffer with a pH = 8, and $AgNO_3$ in a M:L = 2:1 in D) DMF, E) DEF) AND F) DMA. The IR spectrum of G) the tetrazole linker is shown in black.

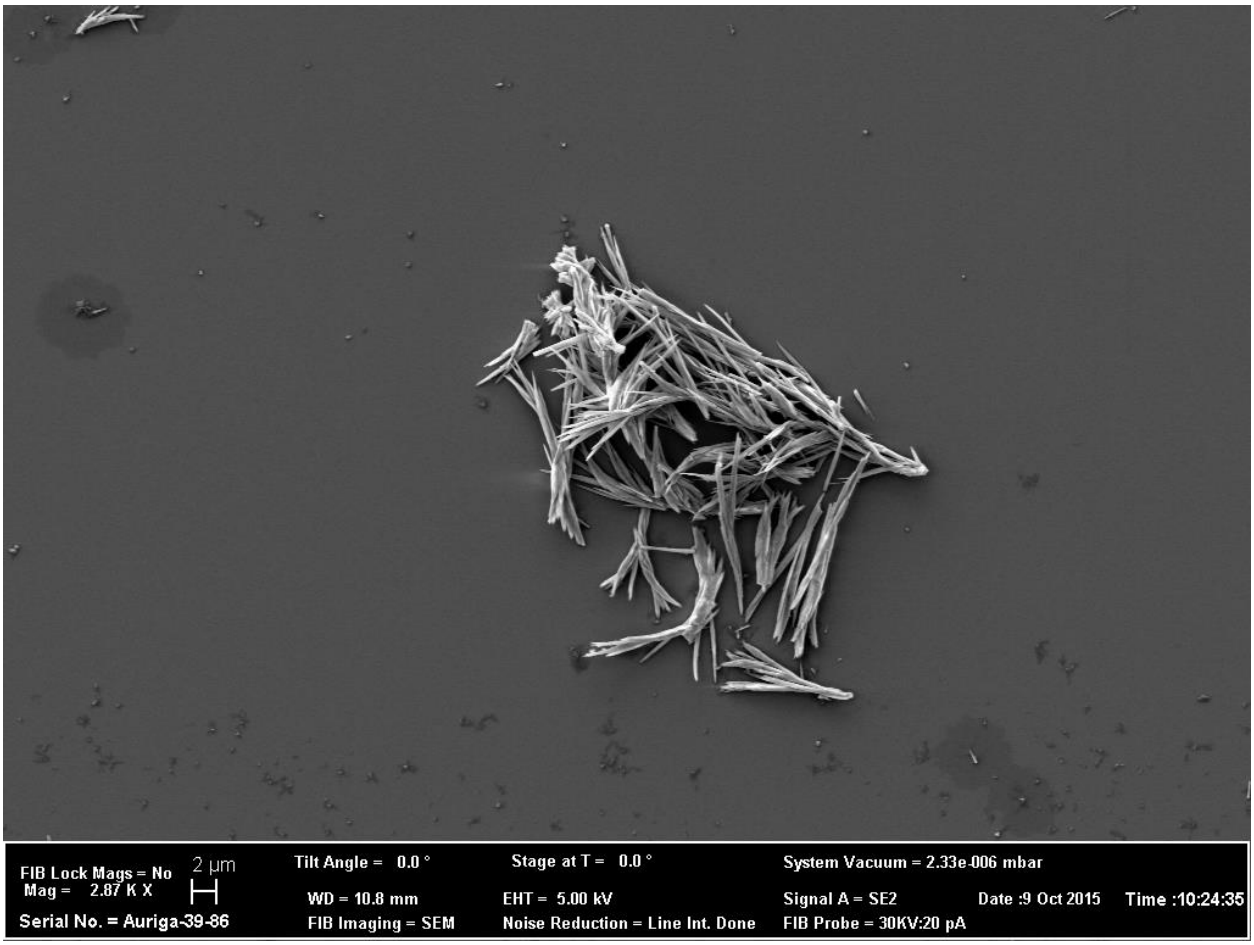

Figure 3.5. SEM image of a copper-based sample that formed nanorods under solvo-thermal conditions. The PXRD pattern for this sample is shown in Figure 3.3.B.

SAXS measurements on this sample and two others failed due to an instrumentation failure, but future studies will examine the mechanism of nucleation, crystal growth, and the kinetics of these reactions.

Because of the propensity for gel formation in protic or amide solvent/water combinations, it was surmised that a more intrinsically basic solvent system, like pyridine, could be a better route to mitigate gel formation and prepare a crystalline solid. Test reactions were carried out with Cu, Ni, Co, and Ag salts, and of these, only samples prepared from $CuSO_4 \cdot 5H_2O$ in a in pyridine/H_2O solvent combinations formed single crystals. The Cu^{II} center crystallized in an octahedral geometry and was bound by two tetrazole ligands and two pyridine molecules in the equatorial positions, and two coordinated water molecules in the axial position (Figure 3.6.B). Within each layer, the ligands formed linear chains with the metal, and packed into 2D sheets by π-π stacking of the pyridine molecules (Figure 3.6.C). The crystals nucleate and grow in such a manner that they form flower-like polycrystalline clusters in which each of the flower “petals” are plate-like single crystals (Figure 3.6.D and 3.6.E).

Several conditions formed this exact same product but no crystals formed from any metal but copper. Other solvents like 2-picoline and 2,6-lutidine were investigated to see if other structures could be prepared, as pyridine is a much stronger donor relative to its functionalized derivatives, and its binding to the metal likely drives the formation of 2D sheets rather than 1D tubes. A trials were carried out with these two solvents but unfortunately poor solubility of either of these solvents in limited their use in MONT reactions. No crystalline solids were obtained and investigations quickly ceased.

Conclusion

Initial attempts to post-synthetically disperse packed MONTs to their discrete form were unsuccessful and further hindered by difficulties with characterization. Transmission electron microscopy was too powerful and amorphized the samples, whereas scanning electron microscopy is better suited for bulk samples and materials with dimensions in the sub-micron regime. Efforts were then put forth to design functionalized ligands that, by steric hindrance, would mitigate MONT aggregation as they form to reduce crystallite size and facilitate the preparation of discrete nanotubes. While only one new functionalized ligand was synthesized due to purification difficulties, the work detailed in this chapter served as framework for guiding new ligand design. Alternative routes are currently being explored to efficiently prepare the organic synthons required, and because of their reliance on classic, well-understood organic reactions, should be a more direct route to prepare the appropriate intermediates. The synthesis of the tetrazole ligand resulted in a few powder crystalline samples that may serve as model compounds for exploring the utility of small-angle X-ray scattering as a primary characterization tool for new MONTs. Though the work detailed in this chapter did not culminate in the preparation of a library of new ligands or discrete metal-organic nanotubes, this work serves as a foundation for future directions.

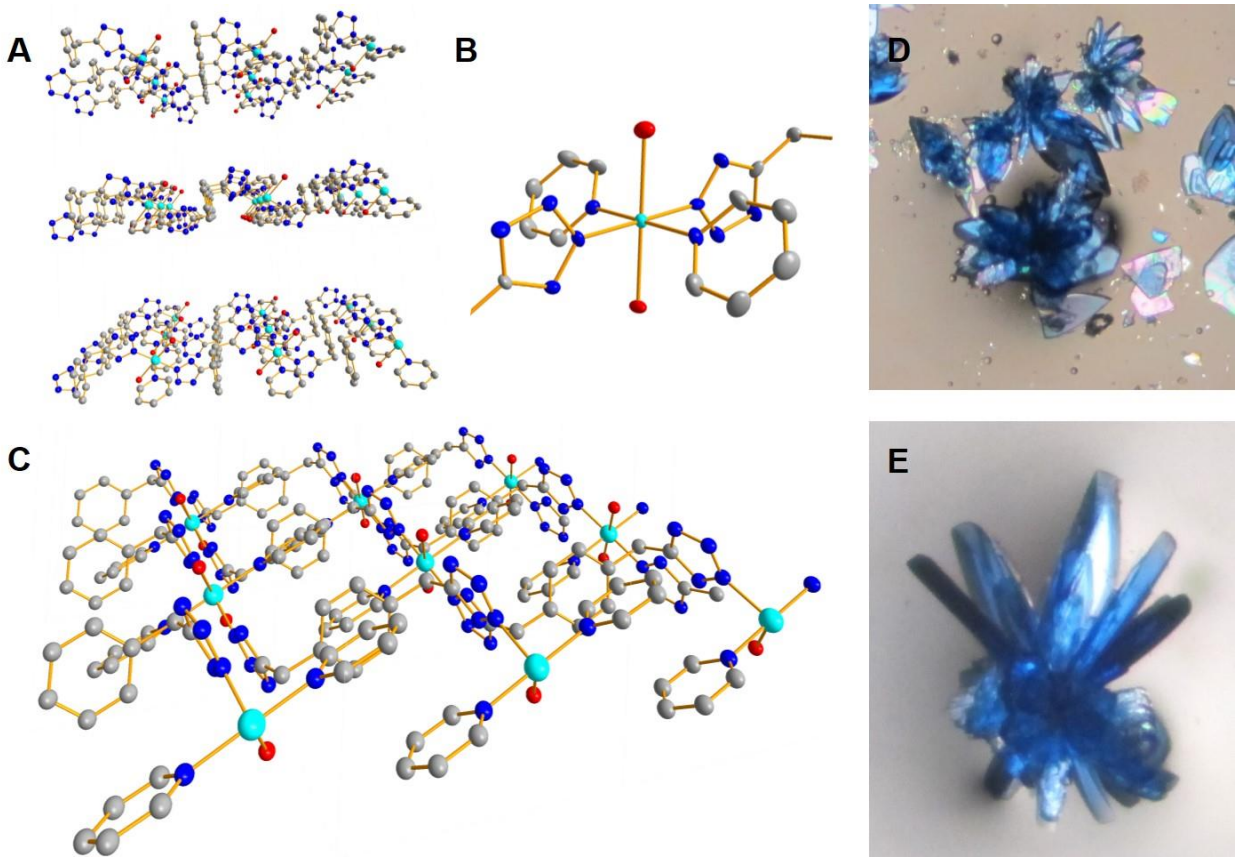

Figure 3.6. Reaction of the tetrazole ligand with $CuSO_4 \cdot 5H_2O$ in pyridine resulted in the formation of A) a 2D sheets that stack into a 3D crystal. B) The ligand and pyridine bind to Cu in an octahedral geometry in which C) the tetrazole ligands form linear chains and pack into 2D sheets by π-π stacking of the pyridine rings. The crystals form D and E) flower-like blue crystals in which each of the "petals" are single-crystals suitable for SCXRD.

Experimental

The compounds 1,2,4-triazole-1-propanenitrile (**2**), 1,4-bis((4H-1,2,4-triazol-4-yl)methyl)benzene (**3**), 1,3-bis((4H-1,2,4-triazol-4-yl)methyl)benzene (**4**), [Ag2(1,4-bis((4H-1,2,4-triazol-4-yl)methyl)benzene)$(NO_3)_2$] • NMP, and (E)-N'-((E)-(dimethylamino)methylene)-N,N-dimethylformohydrazonamide (**6**) were all prepared as previously reported.[1f, 12] All other reagents were purchased from commercial vendors and used without purification. Solution ^{1}H and ^{13}C spectra were recorded at ambient temperature on either a Varian Mercury 300 MHz or Varian VNMRS 500 MHz, narrow-bore broadband system, and the chemical shifts were referenced to the residual solvent. All mass spectrometry analyses were conducted at the Mass Spectrometry Center located in the Department of Chemistry at the University of Tennessee, Knoxville. The DART/MS analyses were performed using a JEOL AccuTOF-D time-of-flight (TOF) mass spectrometer with a DART (direct analysis in real time) ionization source from JEOL USA, Inc (Peabody, MA, USA). The ESI/MS analyses were performed using a QSTAR Elite quadrupole time-of-flight (QTOF) mass spectrometer with an electrospray ionization source from AB Sciex (Concord, Ontario, Canada). Sample solutions for mass spectrometry were prepared in either acetonitrile, acetonitrile/water, ethanol, or ethanol/water combinations. Infrared spectra were collected on a Thermo Scientific Nicolet iS10 with a Smart iTR accessory for attenuated total reflectance.

Synthesis of 4-(4-bromophenyl)-4H-1,2,4-triazole (7). To a 50 mL round bottom flask, 7.17 g (0.042 mol) 4-bromoaniline and 25.47 g (0.118 mol) (E)-N'-((E)-

(dimethylamino)methylene)-N,N-dimethylformohydrazonamide hydrochloride were added and flushed with N_2 for 10 min prior to the addition of 12.5 mL pyridine. The mixture was stirred at room temperature to dissolve the reagents before addition of the flask to an oil bath pre-heated to 115 °C. The starting material 4-bromoaniline was fully consumed after 1 h and the mixture was allowed to cool to room temperature over 2 hours. The pure product was obtained by diluting the reaction mixture with water, filtering over a coarse frit, and washing the white powder three times with diethyl ether and drying under reduced pressure (8.74 g, 93% yield). ^{1}H NMR (DMSO-d_6, 300.1 MHz): σ 9.14 (s, 2H), 7.77 (d, 2H), 7.71 (D, 2H). ^{13}C (DMSO-d_6, 125.67 MHz): σ 141.25, 133.27, 132.78, 123.20, 120. 55. IR (neat): 3130, 3108, 1682, 1521, 1503, 1485, 1452, 1407, 1371, 1312, 1284, 1264, 1220, 1103, 1089, 1069, 1018, 993, 949, 868, 835, 814, 721, 704, 673, 649 cm^{-1}. DART/MS (*m/z*): $[M+H]^+$ 223.99 (found), 223.97 (calculated).

Synthesis of 4-(4-(4,4,5,5-tetramethyl-1,3,2-dioxaborolan-2-yl)phenyl)-4H-1,2,4-triazole (9). To a 100 mL round bottom flask, 503 mg (2.24 mmol) **7**, 630 mg (2.48 mmol) bis(pinacolato)diboron, 691 mg potassium acetate (7.04 mmol), and 95 mg (0.130 mmol, 5 mol%) were added, evacuated and backfilled with N_2 three times prior to the addition of 25 mL anhydrous dioxane that had been purged with N_2 for at least 30 min. The mixture was stirred for 1 min at room temperature before addition of the flask to an oil bath pre-heated to 100 °C. The starting material was fully consumed after 1 h and the mixture was allowed to cool to room temperature, diluted with ethyl acetate, and filtered over celite. The filtrate was collected, solvent removed, and the product was purified via flash

chromatography (5% MeOH in CH_2Cl_2) and subsequent recrystallization from ethyl acetate to afford the pure, tan powder (268 mg, 44% yield). ^{1}H NMR ($CDCl_3$, 499.74 MHz): σ 8.54 (s, 2H), 7.95 (d, 2H), 7.39 (D, 2H), 1.35 (s, 12H). ^{13}C ($CDCl_3$, 125.67 MHz): σ 141.12, 136.79, 135.85, 120.96, 84.34, 24.85. IR (neat) 3101, 2982, 1609, 1579, 1529, 1503, 1418, 1398, 1368, 1358, 1333, 1281, 1236, 1212, 1170, 1142, 1111, 1099, 1083, 1024, 996, 966, 948, 888, 861, 850, 824, 736, 668, 650, 629 cm^{-1}.

Synthesis of 2-methoxy-1,4-dimethylbenzene (11). To a 250 mL round bottom flask, 10.00 g (81.9 mmol) 2,5-dimethylphenol and 5.56 g (99.1 mmol) potassium hydroxide were dissolved in 100 mL acetone and heated to 50 °C. The mixture was stirred at this temperature for 5 min to dissolve the reagents before slow addition of 6.2 mL methyl iodide (14.14 g, 99.6 mmol), and within one minute a white precipitate began to crash out of solution. The reaction was left to stir overnight before cooling to room temperature. The solvent was removed *in vacuo*, diluted with water, and the product was extracted with dichloromethane three times, dried over magnesium sulfate, filtered, and concentrated to a yellow liquid. The product was purified by vacuum distillation to afford a colorless liquid. (10.9 g, 98% yield). ^{1}H NMR ($CDCl_3$, 300.1 MHz): σ 7.29 (d, 1H), 6.95 (d, 1H), 6.91 (s, 1H). ^{13}C (DMSO-d_6, 75 MHz): σ 157.5, 139.9, 131.1, 126.4, 121.23, 111.6, 55.7, 33.2, 28.3 ppm. IR (neat): 2922, 1704, 1616, 1585, 1509, 1464, 1408, 1377, 1309, 1285, 1268, 1254, 1207, 1190, 1153, 1131, 1043, 989, 921, 844, 802, 763, 714, 721 cm^{-1}.

Synthesis of 1,4-bis(bromomethyl)-2-methoxybenzene (12). The starting material, 50 mg (0.367 mmol) 2-methoxy-1,4-dimethylbenzene, was dissolved in 3 mL carbon tetrachloride and bubbled with N_2 for 45 min. A clean, dry 250 mL round bottom flask was charged with 122 mg (0.685 mmol) *N*-bromosuccinimide (NBS) and 5 mg (0.0304 mmol) azobisisobutyronitrile (AIBN), evacuated then backfilled with N_2 three times to remove air. The starting material solution was transferred to the reaction flask under flow of nitrogen, then heated to 78 °C. The starting material was consumed within an hour, the reaction mixture was diluted with hexanes, the succinimide byproduct was filtered off, and the solvent removed *in vacuo*. The crude solid was purified by gradient elution column chromatography using 1-4% ethyl acetate in hexanes. A minor impurity could be seen on the TLC plate and in the NMR spectra (41 mg, 38% yield). ^{1}H NMR (DMSO-d_6, 300.1 MHz): σ 7.30 (d, 1H), 6.98 (d, 1H), 6.91 (s, 1H) 4.54 (s, 2H), 4.47 (s, 2H), 3.92 (s, 3H). ^{13}C (DMSO-d_6, 125.67 MHz): σ 157.53, 139.86, 131.13, 126.44, 121.23, 111.57, 55.68, 33.25, 28.34. IR (neat): 3012, 2936, 2837, 1591, 1450, 1432, 1316, 1288, 1212, 1190, 1162, 1125, 1069, 1017, 983, 948, 890, 860, 802, 733, 701, 665, 650, 634 cm^{-1}.

Synthesis of 1-methoxy-3,5-dimethylbenzene (13). To a 500 mL round bottom flask, 20.01 g (0.164 mol) 3,5-dimethylphenol and 11.21 g (0.199 mol) potassium hydroxide were dissolved in 250 mL acetone and heated to 50 °C. The mixture was stirred at this temperature for 5 min to dissolve the reagents before slow addition of 12 mL methyl iodide (27.4 g, 0.193 mol), and within one minute a white precipitate began to crash out of solution. The reaction was left to stir overnight before cooling to room temperature. The

solvent was removed *in vacuo*, diluted with water, and the product was extracted with dichloromethane three times, dried over magnesium sulfate, filtered, and concentrated to a yellow liquid. The product was purified by vacuum distillation to afford a colorless liquid. (21.20 g, 95% yield). ^{1}H NMR ($CDCl_3$, 499.74 MHz): σ 6.62 (s, 1H), 6.56 (s, 2H), 3.79 (s, 3H), 2.31 (s, 6H) ppm. ^{13}C ($CDCl_3$, 125.67 MHz): σ 159.6, 139.2, 122.4, 111.6, 55.1, 21.4 ppm. IR (neat): 2919, 2836, 1704, 1614, 1596, 1465, 1377, 1465, 1377, 1323, 1295, 1193, 1167, 1151, 1071, 993, 953, 917, 868, 828, 688 cm^{-1}.

Synthesis of 1,3-bis(bromomethyl)-5-methoxybenzene (14). The starting material, 3.01 g (22.1 mmol) 1-methoxy-3,5-dimethylbenzene, was dissolved in 110 mL carbon tetrachloride and bubbled with N_2 for 45 min. A 250 mL round bottom flask was charged with 8.23 g (46.2 mmol) *N*-bromosuccinimide (NBS) and 181 mg (1.10 mmol) azobisisobutyronitrile (AIBN) evacuated then backfilled with N_2 three times to remove air. The starting material solution was transferred to the reaction flask under flow of nitrogen, then heated to 78 °C. The starting material was consumed within an hour, the reaction mixture was diluted with hexanes, the succinimide byproduct was filtered off, and the solvent removed *in vacuo*. The crude solid was flushed through a silica gel plug with 5% ethyl acetate in hexanes, the filtrate was collected, concentrated to a yellow oil, and left to crystallize over 5 days. The colorless, needle crystals were collected by rinsing with hexanes and dried under high vacuum. (1.47 g, 22% yield). TLC of the filtrate confirmed a large amount of residual product and monobrominated impurity. ^{1}H NMR ($CDCl_3$, 499.74 MHz): σ 7.00 (s, 1H), 6.86 (s, 2H), 4.43 (s, 4H), 3.82 (3H) ppm. ^{13}C ($CDCl_3$, 125.67

MHz): σ 160.4, 140.0, 122.2, 115.1, 55.8, 33.2 ppm. IR (neat): 3027, 2964, 2935, 2837, 1597, 1462, 1433, 1334, 1299, 1205, 1196, 1164, 1155, 1124, 1110, 995, 981, 944, 869, 853, 694, 632, cm^{-1}.

Synthesis of 1,4-dimethyl-2-propoxybenzene (15). To a 500 mL round bottom flask, 5.02 g (41.1 mmol) 2,5-dimethylphenol and 2.78 g (49.5 mmol) potassium hydroxide were dissolved in 200 mL acetone and heated to 50 °C. The mixture was stirred at this temperature for 5 min to dissolve the reagents before slow addition of 3.85 mL 1-bromopropane (5.21 g, 42.3 mmol), and within one minute a white precipitate began to crash out of solution. The reaction was left to stir overnight before cooling to room temperature. The solvent was removed *in vacuo*, diluted with water, and the product was extracted with dichloromethane three times, dried over magnesium sulfate, filtered, and concentrated to a yellow liquid. The product was purified by vacuum distillation to afford a colorless liquid. (11.5 g, 94% yield). ^{1}H NMR ($CDCl_3$, 300.1 MHz): σ 7.00 (d, 1H), 6.66 (d, 1H), 6.63 (s, 1H), 3.90 (t, 2H), 2.17 (s, 3H), 1.81 (m, 2H), 1.25 (s, 3H), 1.04 (t, 3H). ^{13}C ($CDCl_3$, 75 MHz): σ 157.07, 136.39, 130.22, 123.62, 120.51, 112.00, 53.77, 31.71, 30.91, 29.25, 22.75, 21.38, 15.74, 10.65. IR (neat): 2963, 2923, 2877, 1614, 1586, 1508, 1457, 1413, 1389, 1308, 1263, 1209, 1159, 1130, 1067,1048, 1028, 1005, 977, 920, 843, 801, 765, 715 cm^{-1}.

Synthesis of (2,5-dimethylphenoxy)trimethylsilane (16). To a 250 mL round bottom flask, 509 mg (4.17 mmol) 2,5-dimethylphenol and 1.00 mL (12.4 mmol) pyridine were

dissolved in 10 mL dichloromethane and cooled to 0 °C before slow addition of 1.5 mL trimethylsilane chloride (1.28 g, 11.8 mmol), and within one minute a white precipitate began to crash out of solution. The reaction stirred for 15, then warmed to room temperature, diluted with water, then extracted three times with dichloromethane, dried over magnesium sulfate before cooling to room temperature. The solvent was removed *in vacuo*, diluted with water, and the product was extracted with dichloromethane three times, dried over magnesium sulfate, filtered and concentrated to a colorless liquid with white solid. The mixture was diluted with hexanes and filtered over alumina to afford the product as a pure, colorless liquid. (468 mg, 58% yield). ^{1}H NMR ($CDCl_3$, 499.74 MHz): σ 7.02 (d, 1H), 6.70 (d, 1H), 7.71, 2.28 (s, 3H), 2.15 (s, 2H), 0.27 (s, 9H). ^{13}C ($CDCl_3$, 125.67 MHz): σ 153.41, 136.31, 130.54, 125.68, 121.95, 119.81, 21.05, 16.14, 0.47. IR (neat): 2958, 1616, 1580, 1507, 1410, 1274, 1251, 1157, 1127, 1002, 953, 865, 839, 801, 752, 692 cm^{-1}.

Synthesis of (3,5-dimethylphenoxy)trimethylsilane (17). To a 250 mL round bottom flask, 509 mg (4.17 mmol) 2,5-dimethylphenol and 1.00 mL (12.4 mmol) pyridine were dissolved in 10 mL dichloromethane and cooled to 0 °C before slow addition of 1.5 mL trimethylsilane chloride (1.28 g, 11.8 mmol), and within one minute a white precipitate began to crash out of solution. The reaction stirred for 15, then warmed to room temperature, diluted with water, then extracted three times with dichloromethane, dried over magnesium sulfate before cooling to room temperature. The solvent was removed *in vacuo*, diluted with water, and the product was extracted with dichloromethane three

times, dried over magnesium sulfate, filtered and concentrated to a colorless liquid with white solid. The mixture was diluted with hexanes and filtered over alumina to afford the product as a pure, colorless liquid. (468 mg, 58% yield). ^{1}H NMR ($CDCl_3$, 499.74 MHz): σ 7.02 (d, 1H), 6.70 (d, 1H), 7.71, 2.28 (s, 3H), 2.15 (s, 2H), 0.27 (s, 9H). ^{13}C ($CDCl_3$, 125.67 MHz): σ 153.41, 136.31, 130.54, 125.68, 121.95, 119.81, 21.05, 16.14, 0.47.

Synthesis of 4,4'-((2-methoxy-1,4-phenylene)bis(methylene))bis(4H-1,2,4-triazole) (18). In a clean, dry 10 mL round bottom flask 52 mg (0.178 mmol) 1,4-bis(bromomethyl)-2-methoxybenzene (12) and 48 mg (0.393 mmol) 3-(1H-1,2,4-triazol-1-yl)propanenitrile were dissolved in 3 mL acetonitrile and refluxed overnight. The solvent was removed *in vacuo* to afford a yellow oil, to which 31 mg (0.551 mmol) potassium hydroxide was added and dissolved in 2 mL water and allowed to stir overnight at room temperature. Solvent was removed and ethyl acetate was employed to pull off residual impurities. The off-white solid was dried under high vacuum to afford the final ligand with salt impurities. Quantities isolated were too small for purification and impurities limited accurate yield determination. ^{1}H NMR (DMSO-d_6, 300.1 MHz): σ 8.64 (s, 2H), 8.49 (s, 3H), 7.19 (d, 1H), 7.11 (s, 1H), 6.86 (d, 1H), 5.26 (s, 2H), 5.17 (s, 2H), 3.82 (s, 2H). IR (neat): 3405, 2162, 2050, 1979, 1635, 1539, 1402, 1267, 1184, 1402, 1267, 1184, 1076, 1033, 638 cm^{-1}.

Synthesis of 4,4'-((5-methoxy-1,3-phenylene)bis(methylene))bis(4H-1,2,4-triazole) (19). In a clean, dry 50 mL round bottom flask 502 mg (1.72 mmol) 1,3-bis(bromomethyl)-

5-methoxybenzene (14) and 847 mg (6.94 mmol) 3-(1H-1,2,4-triazol-1-yl)propanenitrile were dissolved in 15 mL acetonitrile and refluxed overnight. The mixture was cooled to room temperature and white solid crashed out of solution. The mixture was diluted with diethyl ether, the solid collected, dried, then combined with 273 mg (4.86 mmol) potassium hydroxide, dissolved in 15 mL ethanol and refluxed overnight. The reaction mixture was cooled to room temperature, solid crashed out and was filtered. The filtrate was collected, concentrated to a white solid, and dried under high vacuum to afford the final ligand with salt impurities. The product was further purified by Soxhlet extraction over 40 h. (154 mg, 33% overall yield). ^{1}H NMR (DMSO-d_6, 499.74 MHz): σ 8.61 (s, 4H), 6.87 (s, 2H), 6.85 (s, 1H), 4.28 (s, 4H), 3.73 (s, 3H) ppm. ^{13}C (DMSO-d_6, 125.67 MHz): σ 160.2, 143.7, 139.2, 119.6, 113.6, 55.8, 47.6 ppm. IR (neat): 3091, 3035, 2941, 2848, 1787, 1662, 1612, 1599, 1530, 1473, 1456, 1439, 1376, 1350, 1333, 1299, 1220, 1180, 1160, 1064, 994, 975, 951, 942, 910, 888, 833, 755, 691, 658, 647, 626 cm^{-1}.

Synthesis of 2,2'-(1,4-phenylene)diacetonitrile (21). In a clean, dry 1L round bottom flask 25.00 g (0.143 mol) 1,4-bis(chloromethyl)benzene and 19.30 g (0.429) sodium cyanide were dissolved in 500 mL acetonitrile and refluxed for 3 d. The orange suspension was cooled to room temperature, the solvent removed *in vacuo*, the residue immersed in dichloromethane, filtered, and the orange filtrate concentrated to an orange solid that required no further purification. The solid was dried under high vacuum. (21.19 g, 95% yield). ^{1}H NMR ($CDCl_3$, 499.74 MHz): σ 7.35 (s, 3H), 3.75 (s, 4H) ppm. ^{13}C ($CDCl_3$, 125.67 MHz): 130.1, 128.8, 117.6, 23.4 ppm. IR (neat): 2938, 2918, 2248, 1931,

1709, 1518, 1424, 1413, 1263, 1222, 1191, 1127, 1021, 974, 944, 931, 803, 782, 751, 736 cm^{-1}.

Synthesis of 1,4-bis((2H-tetrazol-5-yl)methyl)benzene (22). In a clean, dry 1L round bottom flask 8.48 g (0.513 mol) 2,2'-(1,4-phenylene)diacetonitrile, 20.57 g (0.316 mmol) sodium azide, and 43.37 g (0.315 mol) trimethylamine hydrochloride were dissolved in 500 mL toluene and refluxed for 3 d with vigorous. The suspension was cooled to room temperature, about half the solvent was removed *in vacuo*, and the remaining mixture was washed 150 mL 1 M KOH solution. The aqueous phase was isolated, filtered over celite to remove residual solid, then acidified with a large excess of 1 M HCl solution until a pH = 1 was achieved. The white precipitate was collected by vacuum filtration, washed with diethyl ether, and dried under high vacuum to afford the pure product. (9.20 g, 70% yield). ^{1}H NMR ($CDCl_3$, 499.74 MHz): σ 7.23 (s, 3H), 4.25 (s, 4H) ppm. ^{13}C ($CDCl_3$, 125.67 MHz): 155.3, 134.7, 129.0, 28.6 ppm. IR (neat): 3006, 2860, 2714, 2608, 2482, 1580, 1517, 1406, 1270, 1252, 1213, 1111, 1088, 1052, 991, 921, 831, 783, 748, 716, 670, 512 cm^{-1}.

Preparation of pH = 5.38 solution. A stock solution of 0.25 M HNO_3 was prepared, and 40 µL was diluted to 100 mL in a volumetric flask.

Preparation of pH = 8 buffer solution. Aqueous stock solutions of 0.1 M HCl and 0.1 tris(hydroxymethyl)aminomethane were prepared, and 58.4 mL 0.1 M HCl and 41.6 mL tris(hydroxymethyl)aminomethane solution were mixed in a 100 mL volumetric flask.

Synthesis of sample 3.3.A. 8.9 mg (0.0366 mmol) **22** was dissolved in 2 mL DMA and heated to 85 °C for 5 min to dissolve. In a separate vial, 18 mg (0.0732 mmol) $CuSO_4 \cdot 5H_2O$ was dissolved in 1 mL aqueous HNO_3 at a pH = 5.38. The aqueous solution was transferred to the ligand solution and blue solid immediately crashed out of solution. The mixture was swirled and heated to 85 °C over two weeks. Blue microcrystalline solid formed, was collected, and rinsed with acetone and dried in air.

Synthesis of sample 3.3.B. 8.9 mg (0.0366 mmol) **22** and 4 mg potassium hydroxide were dissolved in 2 mL water and stirred to dissolve. In a separate vial, 18 mg (0.0732 mmol) $CuSO_4 \cdot 5H_2O$ was dissolved in 1 mL aqueous buffer set to a pH = 8. The aqueous solution was transferred to the ligand solution and blue solid immediately crashed out of solution. The mixture was swirled and heated to 85 °C over two weeks. Blue microcrystalline solid formed, was collected, and rinsed with acetone and dried in air.

Synthesis of sample 3.3.C. 8.9 mg (0.0366 mmol) **22** and 4 mg potassium hydroxide were dissolved in 2 mL water and stirred to dissolve. In a separate vial, 36 mg (0.146 mmol) $CuSO_4 \cdot 5H_2O$ was dissolved in 1 mL aqueous buffer set to a pH = 8. The aqueous solution was transferred to the ligand solution and blue solid immediately crashed out of solution. The mixture was swirled and heated to 85 °C over two weeks. Blue microcrystalline solid formed, was collected, and rinsed with acetone and dried in air.

Synthesis of sample 3.3.D. 8.9 mg (0.0366 mmol) **22** was dissolved in 2 mL DMF and stirred to dissolve. In a separate vial, 12 mg (0.0732 mmol) $AgNO_3$ was dissolved in 1 mL H_2O and stirred to dissolve. Both solutions were cooled to 0 °C over 45 minutes, then mixed at this temperature. A white suspension immediately crashed out of solution. The mixture was swirled and heated to 85 °C, and after 3 h, white microcrystalline solid formed.

Synthesis of sample 3.3.E. 8.9 mg (0.0366 mmol) **22** was dissolved in 2 mL DMF and stirred to dissolve. In a separate vial, 12 mg (0.0732 mmol) $AgNO_3$ was dissolved in 1 mL H_2O and stirred to dissolve. Both solutions were cooled to 0 °C over 45 minutes, then mixed at this temperature. A white suspension immediately crashed out of solution. The mixture was swirled and heated to 85 °C, and after 3 h, white microcrystalline solid formed.

Synthesis of sample 3.3.F. 8.9 mg (0.0366 mmol) **22** was dissolved in 2 mL DMF and stirred to dissolve. In a separate vial, 12 mg (0.0732 mmol) $AgNO_3$ was dissolved in 1 mL H_2O and stirred to dissolve. Both solutions were cooled to 0 °C over 45 minutes, then mixed at this temperature. A white suspension immediately crashed out of solution. The mixture was swirled and heated to 85 °C, and after 3 h, white microcrystalline solid formed.

References

1. (a) Adarsh, N. N.; Dîrtu, M. M.; Naik, A. D.; Léonard, A. F.; Campagnol, N.; Robeyns, K.; Snauwaert, J.; Fransaer, J.; Su, B. L.; Garcia, Y., Single-Walled Metal–Organic Nanotube Built from a Simple Synthon. *Chem. Eur. J.* **2015,** *21*, 4300-4307; (b) Cao, G.-J.; Liu, J.-D.; Zhuang, T.-T.; Cai, X.-H.; Zheng, S.-T., A polyoxometalate-organic supramolecular nanotube with high chemical stability and proton-conducting properties. *Chem. Commun.* **2015,** *51*, 2048-2051; (c) Dai, F.; He, H.; Sun, D., A Metal−Organic Nanotube Exhibiting Reversible Adsorption of $(H_2O)_{12}$ Cluster. *J. Am. Chem. Soc.* **2008,** *130*, 14064-14065; (d) Fei, Z.; Zhao, D.; Geldbach, T. J.; Scopelliti, R.; Dyson, P. J.; Antonijevic, S.; Bodenhausen, G., A Synthetic Zwitterionic Water Channel: Characterization in the Solid State by X-ray Crystallography and NMR Spectroscopy. *Angew. Chem. Int. Ed.* **2005,** *44*, 5720-5725; (e) Liu, W.-T.; Ou, Y.-C.; Xie, Y.-L.; Lin, Z.; Tong, M.-L., Photoluminescent Metal-Organic Nanotubes via Hydrothermal in Situ Ligand Reactions. *Eur. J. Inorg. Chem.* **2009,** *2009*, 4213-4218; (f) Murdock, C. R.; Jenkins, D. M., Isostructural Synthesis of Porous Metal–Organic Nanotubes. *J. Am. Chem. Soc.* **2014,** *136*, 10983-10988; (g) Otsubo, K.; Wakabayashi, Y.; Ohara, J.; Yamamoto, S.; Matsuzaki, H.; Okamoto, H.; Nitta, K.; Uruga, T.; Kitagawa, H., Bottom-up realization of a porous metal–organic nanotubular assembly. *Nat. Mater.* **2011,** *10*, 291-295; (h) Ren, S.-B.; Yang, X.-L.; Zhang, J.; Li, Y.-Z.; Zheng, Y.-X.; Du, H.-B.; You, X.-Z., An infinite photoluminescent coordination nanotube $[CuSCN(L)]\bullet(DMF)_{0.5}$. *CrystEngComm* **2009,** *11*, 246-248; (i) Thuéry, P., A Highly Adjustable Coordination System: Nanotubular and Molecular Cage Species in Uranyl Ion Complexes with Kemp's Triacid. *Cryst. Growth Des.* **2014,** *14*, 901-904; (j) Tseng, T.-W.; Luo, T.-T.; Su, C.-C.; Hsu, H.-H.; Yang, C.-I.; Lu, K.-L., An unusual cobalt(ii)-based single-walled metal-organic nanotube. *CrystEngComm* **2014,** *16*, 2626-2633; (k) Unruh, D. K.; Gojdas, K.; Libo, A.; Forbes, T. Z., Development of Metal–Organic Nanotubes Exhibiting Low-Temperature, Reversible Exchange of Confined "Ice Channels". *J. Am. Chem. Soc.* **2013,** *135*, 7398-7401; (l) Zhang, G.-L.; Zhou, L.-P.; Yuan, D.-Q.; Sun, Q.-F., Bottom-Up Construction of Mesoporous Nanotubes from 78-Component Self-Assembled Nanobarrels. *Angew. Chem. Int. Ed.* **2015,** *54*, 9844-9848; (m) Zhang, Q.; Geng, A.; Zhang, H.; Hu, F.; Lu, Z.-H.; Sun, D.; Wei, X.; Ma, C., An Independent 1D Single-Walled Metal–Organic Nanotube Transformed from a 2D Layer Exhibits Highly Selective and Reversible Sensing of Nitroaromatic Compounds. *Chem. Eur. J.* **2014,** *20*, 4885-4890.
2. (a) Fukino, T.; Joo, H.; Hisada, Y.; Obana, M.; Yamagishi, H.; Hikima, T.; Takata, M.; Fujita, N.; Aida, T., Manipulation of Discrete Nanostructures by Selective Modulation of Noncovalent Forces. *Science* **2014,** *344*, 499-504; (b) Yamagishi, H.; Fukino, T.; Hashizume, D.; Mori, T.; Inoue, Y.; Hikima, T.; Takata, M.; Aida, T., Metal–Organic Nanotube with Helical and Propeller-Chiral Motifs Composed of a C_{10}-Symmetric Double-Decker Nanoring. *J. Am. Chem. Soc.* **2015,** *137*, 7628-7631.
3. (a) Dürr, A. C.; Schreiber, F.; Kelsch, M.; Dosch, H., Optimized preparation of cross-sectional TEM specimens of organic thin films. *Ultramicroscopy* **2003,** *98*, 51-55; (b)

Mayer, J.; Giannuzzi, L. A.; Kamino, T.; Michael, J., TEM Sample Preparation and FIB-Induced Damage. *MRS Bull.* **2007,** *32*, 400-407.
4. (a) Cenker, Ç. Ç.; Bomans, P. H. H.; Friedrich, H.; Dedeoğlu, B.; Aviyente, V.; Olsson, U.; Sommerdijk, N. A. J. M.; Bucak, S., Peptide nanotube formation: a crystal growth process. *Soft Matter* **2012,** *8*, 7463-7470; (b) Etampawala, T.; Mull, D. L.; Keum, J. K.; Jenkins, D. M.; Dadmun, M., Insights into the Morphology and Kinetics of Growth of Silver Metal–Organic Nanotubes. *Cryst. Growth Des.* **2016,** *16*, 1395-1403; (c) Graveland-Bikker, J. F.; Fritz, G.; Glatter, O.; De Kruif, C. G., Growth and structure of α-lactalbumin nanotubes. *J. Appl. Crystallogr.* **2006,** *39*, 180-184; (d) Landau, M. V.; Vradman, L.; Wang, X.; Titelman, L., High loading TiO_2 and ZrO_2 nanocrystals ensembles inside the mesopores of SBA-15: preparation, texture and stability. *Microporous Mesoporous Mater.* **2005,** *78*, 117-129; (e) Maillet, P.; Levard, C.; Larquet, E.; Mariet, C.; Spalla, O.; Menguy, N.; Masion, A.; Doelsch, E.; Rose, J.; Thill, A., Evidence of Double-Walled Al−Ge Imogolite-Like Nanotubes. A Cryo-TEM and SAXS Investigation. *J. Am. Chem. Soc.* **2010,** *132*, 1208-1209.
5. (a) Demortière, A.; Schaller, R. D.; Li, T.; Chattopadhyay, S.; Krylova, G.; Shibata, T.; dos Santos Claro, P. C.; Rowland, C. E.; Miller, J. T.; Cook, R.; Lee, B.; Shevchenko, E. V., In Situ Optical and Structural Studies on Photoluminesence Quenching in CdSe/CdS/Au Heterostructures. *J. Am. Chem. Soc.* **2014,** *136*, 2342-2350; (b) Hubert, F.; Testard, F.; Thill, A.; Kong, Q.; Tache, O.; Spalla, O., Growth and Overgrowth of Concentrated Gold Nanorods: Time Resolved SAXS and XANES. *Cryst. Growth Des.* **2012,** *12*, 1548-1555; (c) Morita, T.; Hatakeyama, Y.; Nishikawa, K.; Tanaka, E.; Shingai, R.; Murai, H.; Nakano, H.; Hino, K., Multiple small-angle X-ray scattering analyses of the structure of gold nanorods with unique end caps. *Chem. Phys.* **2009,** *364*, 14-18; (d) Tsao, C.-S.; Chuang, C.-M.; Chen, C.-Y.; Huang, Y.-C.; Cha, H.-C.; Hsu, F.-H.; Chen, C.-Y.; Tu, Y.-C.; Su, W.-F., Reaction Kinetics and Formation Mechanism of TiO2 Nanorods in Solution: An Insight into Oriented Attachment. *J. Phys. Chem. C* **2014,** *118*, 26332-26340.
6. (a) Deng, H.; Grunder, S.; Cordova, K. E.; Valente, C.; Furukawa, H.; Hmadeh, M.; Gándara, F.; Whalley, A. C.; Liu, Z.; Asahina, S.; Kazumori, H.; O'Keeffe, M.; Terasaki, O.; Stoddart, J. F.; Yaghi, O. M., Large-Pore Apertures in a Series of Metal-Organic Frameworks. *Science* **2012,** *336*, 1018-1023; (b) Eddaoudi, M.; Kim, J.; Rosi, N.; Vodak, D.; Wachter, J.; O'Keeffe, M.; Yaghi, O. M., Systematic Design of Pore Size and Functionality in Isoreticular MOFs and Their Application in Methane Storage. *Science* **2002,** *295*, 469-472.
7. Horváth, A., Michael Adducts in the Regioselective Synthesis of N-Substituted Azoles. *Synthesis* **1995,** *1995*, 1183-1189.
8. Zhao, G.; Wang, Z.; Wang, R.; Li, J.; Zou, D.; Wu, Y., Cucurbit[7]uril promoting PdCl2-catalyzed cross-coupling reaction of benzyl halides and arylboronic acids in aqueous media. *Tetrahedron Lett.* **2014,** *55*, 5319-5322.
9. Inés, B.; Moreno, I.; SanMartin, R.; Domínguez, E., A Nonsymmetric Pincer-Catalyzed Suzuki−Miyaura Arylation of Benzyl Halides and Other Nonactivated Unusual Coupling Partners. *J. Org. Chem.* **2008,** *73*, 8448-8451.

10. Burns, M. J.; Fairlamb, I. J. S.; Kapdi, A. R.; Sehnal, P.; Taylor, R. J. K., Simple Palladium(II) Precatalyst for Suzuki−Miyaura Couplings: Efficient Reactions of Benzylic, Aryl, Heteroaryl, and Vinyl Coupling Partners. *Org. Lett.* **2007,** *9*, 5397-5400.
11. Bandgar, B. P.; Bettigeri, S. V.; Phopase, J., Palladium catalyzed ligand-free Suzuki cross-coupling reactions of benzylic halides with aryl boronic acids under mild conditions. *Tetrahedron Lett.* **2004,** *45*, 6959-6962.
12. Bartlett, R. K.; Humphrey, I. R., Transaminations of NN-dimethylformamide azine. *J. Chem. Soc. C* **1967**, 1664-1666.

CHAPTER 4
SYNTHESIS OF A THIOL-TAGGED CYCLIC AMIDOXIME LIGAND TO BIND URANYL ION FOR URANIUM DETECTION USING SERS

Most of the work detailed in this chapter was carried out during the Spring 2014 semester, and was my focus before picking up work on the MONTs project.

The work here was a continuation of the worked carried out by Dr. Chi-Linh Do-Thanh with Dr. Karl Bernstein in a manuscript that was published in 2014:

Bernstein, Karl J.; Do-Thanh, Chi-Linh; Penchoff, Deborah A.; Cramer, S. Alan; Murdock, Christopher R.; Lu, Zheng; Harrison, Robert J.; Camden, Jon P.; Jenkins, David M. “The Synthesis and Spectroscopic Characterization of an Aromatic Uranium Amidoxime Complex.” *Inorg. Chim. Acta*, **2014**, *421*, 374-379.

Abstract

The synthesis of a thiol-tagged cyclic amidoxime ligand for uranium detection was attempted. Our group collaborated with the Camden group at the University of Notre Dame to develop a portable device that can detect the uranyl (UO_2^{2+}) cation at ultra-low concentrations by employing surface-enhanced Raman spectroscopy (SERS). The ability for on-sight detection of highly enriched uranium is highly attractive for global security and monitoring weapons proliferation.

Introduction

The Nuclear Non-Proliferation Treaty (NPT) of 1968 was signed to mitigate nuclear proliferation by encouraging the development of nuclear technology for civilian use.[1] In the 1950s it was widely assumed that there would be 30-35 nuclear weapons states by the turn of the 21st century; currently, there are only 9.[2] Failed attempts by Argentina, Iran,

Syria, and Libya, and the recent success by the North Korean regime to develop a nuclear weapons program, highlight the fact many countries are still attempting to develop their own nuclear arsenals.[1]

The United Nations and the International Atomic Energy Agency work to monitor countries that have signed the NPT and are suspected to be developing a nuclear weapons program.[3] A country that is thought to doing this is subject to UN inspections of uranium enrichment facilities to detect the presence of U^{235}, the isotope that is employed in nuclear weapons. Samples are collected on site and sent to a laboratory for analysis by inductively coupled plasma mass spectrometry (ICP-MS), which allows for differentiation between uranium isotopes.[4] While this analytical method is highly accurate and sensitive, the major limitation is that results are delayed for weeks and this can hinder repercussions following a violation. While rare, smuggling of radioactive material is an additional concern of the international community, and the few instances in which perpetrators have been caught underscores that this continues to be a threat.[5]

The Joint Comprehensive Plan of Action with the Islamic Republic of Iran underscores the need to develop methods to perform on-site inspections to obtain fast and immediate detection of radioactive materials to determine if violations occurred.[6] Portable Raman spectrometer devices have previously been developed for the immediate detection of environmental contaminants[7] and biomarkers,[8] and there is growing interest to apply this to uranium detection and nuclear forensics.[9] Portable devices often employ Raman Spectroscopy as the analyte-identification method of choice owning to the fact

that a portable Raman device is easy to fabricate and each compound gives a signature spectrum.

A more sensitive variation of Raman spectroscopy is surface-enhanced Raman spectroscopy (SERS), a method in which the analyte is chemisorbed or physisorbed to a noble metal surface like Au or Ag.[10] Signal enhancement is typically 10^{6}-10^{7}, and SERS has even allowed for single-molecule detection.[11] Indeed, because of the sensitivity of SERS, our group established a collaboration with the Camden group to develop a SERS-based portable device for uranium detection.

Results and Discussion

Work began to expand upon the Camden and Jenkins groups published in 2014.[9a] A naphthalene-based cyclic amidoxime was synthesized by a simple three-step route outlined in Scheme 4.1.A. The cyclic amidoxime complex was formed by dissolving the ligand with uranyl nitrate hexahydrate, $UO_2(NO_3)_2(H_2O)_6$, in methanol. Crystals formed after slow evaporation over 2 days which allowed for characterization via X-ray crystallography. The ligand and complex were characterized by ^{13}C CP MAS NMR, IR, and Raman spectroscopies and demonstrated the applicability of these methods to characterize the binding of uranium to cyclic amidoxime ligands. In order to apply this system to develop a portable, SERS-based device, synthesis of a tagged-ligand in which an additional functional group, like a thiol or an amine, is incorporated to bind to a metal surface.

Prior to my arrival, an original route was employed in which large quantities of **2**, reasonably quantities of **3**, and a few milligrams of **4**, were prepared, but in low yields (Scheme 4.1.B). During my first few months as a graduate student in the Jenkins group I commenced work to finish the sequence that had been started. Beside the initial bromination step to form 5-bromoacenaphthylene-1,2-dione (**2**), the following two steps to prepare compounds **3** and **4** were modified according to the procedures outlined previously.[12] The thiadiazole dioxide intermediate **4** was prepared by addition of a large excess of acetyl chloride to a solution of **2** and sulfamide, **3**, in refluxing methanol. An instant color change and precipitation of orange solid is observed and the reaction reaches completion over 12 hours. The crude solid can be used in the next step. Molecule **4** is added directly to diethyl glyme and the suspension is heated to 200 °C to evolve SO_2 and afford the dinitrile intermediate **5**, which can be collected by filtration and purified by recrystallization from toluene.

Rather than employ sodium thioethoxide to form the thiol, a Buchwald-Hartwig reaction modified to prepare aromatic thiols was employed to couple triisopropylsilanethiol (TIPS-SH) (**8**) to **5** to form the TIPS-protected thiol, **9**.[13] The product was detected during the first trial reaction, and as the manuscript suggested, a 15% tetrabutylammonium fluoride (TBAF) in THF solution was added to the reaction mixture to deprotect the thiol to form free **6**. Unsuccessful isolation led us to focus on isolating molecule **9**. Though there were a couple more conditions in which the TIPS- protected product could be detected, the initial conditions outlined in the manuscript overall were unsuccessful for catalyzing the reaction, although the molecules synthesized from the

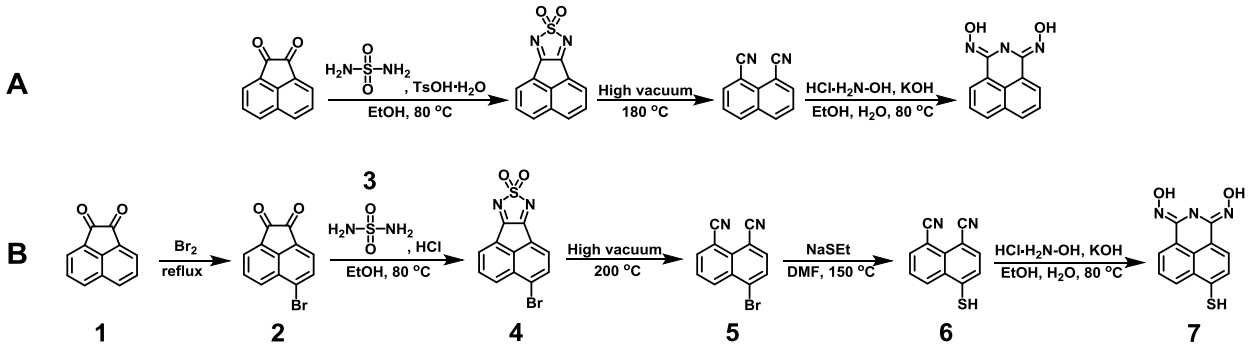

Scheme 4.1. A) Original amidoxime sequence published by the Camden and Jenkins groups and B) the original synthetic pathway to prepare the thiol-tagged cyclic amidoxime.

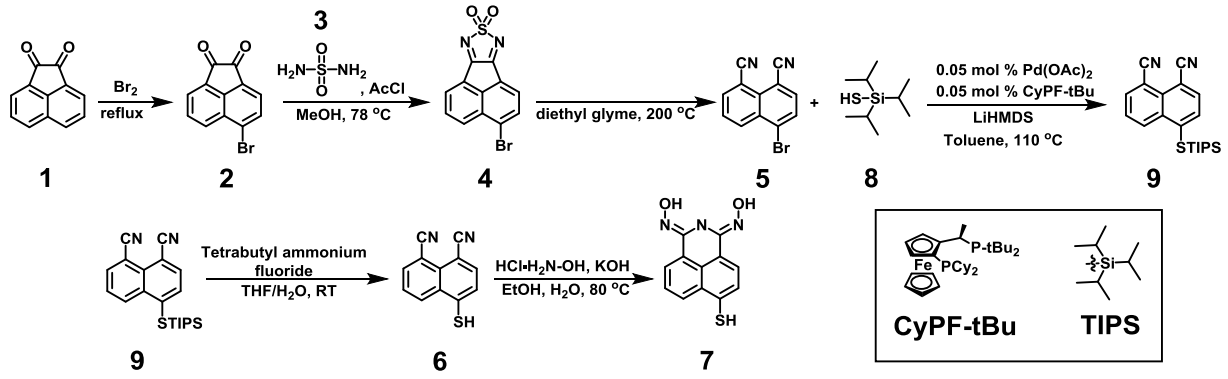

Scheme 4.2. Modified route to prepare the thiol-tagged cyclic amidoxime. Molecules 4 and 5 were prepared according to published procedures.[12]

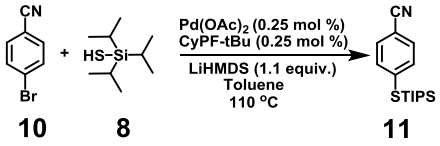

Scheme 4.3. Test reaction to reproduce results from original manuscript by Hartwig and coworkers.

procedure employed were all of functionalized benzene rings. A test reaction with 4-bromonitrile, **10**, and **8** was carried out under the conditions listed in Scheme 4.3 and the product, molecule **11**, was isolated in 39% yield (Scheme 4.3). The proton spectrum showed all the corresponding peaks with correct integration values, but **11** was not fully characterized.

With verification that coupling conditions do indeed work for a smaller ring system, our efforts were directed toward finding the appropriate solvent and temperature combinations to couple TIPS-SH to **5**, and the conditions attempted are listed in Table 4.1. There were a handful of conditions in which the product could be detected in the DART-MSc, but the product was never isolable. The desired product was not detected in the DART-MS for the majority of conditions tested despite solvent, temperature, and catalyst loading adjustments. The next step was to investigate new metal-ligand combinations to overcome the activation barrier for coupling.

Bunte salts, or organic thiosulfate anions, have found use in the commercial production of thiols as they are air stable and odorless.[14] They have been applied as precursors to self-assembled monolayers (SAMs) on Ag surfaces following electrocatalytic cleavage of the sulfite group to form the free thiol in solution.[14] These two critical traits piqued our interest as these salts could be advantageous route to store the ligand prior to preparing the nanoparticles for SERS analysis. Following the procedure outlined by Lukkari and coworkers, test reactions were carried out to couple sodium thiosulfate with molecule **5** using Pd_2dba_3 and the commercially available ligand XPhos (Scheme 4.4). The intermediate **12** was detected in the QSTAR ESI mass spectrometer,

but following reduction with Zn/HCl to obtain the free thiol **6**, the product was unable to be isolated or its presence detected in the reaction mixture. The next focus was to isolate the pure Bunte salt, but because it is an inorganic solid, purification by column chromatography was not feasible and efforts to recrystallize the salt were undertaken. Its limited solubility made purification exceptionally difficult, and after spending a few weeks attempting to crystallize the Bunte salt from polar solvents, the project was put on hold.

Conclusions

Development of a portable, SERS-based device for the rapid and accurate detection of enriched uranium presents a unique challenge to synthetic chemists and spectroscopists. This chapter outlined previous work that demonstrate the binding of UO_2 to a cyclic amidoxime ligand can be readily characterized by spectroscopic methods including ^{13}C CP-MAS NMR, IR, and Raman, and discussed attempted pathways to synthesize a thiol-tagged cyclic amidoxime. While a route that has been classically used to prepare aromatic thiols was previously proposed, my work focused on employing aromatic-thiol/thiosulfate cross-coupling reactions that required less harsh conditions. While the final ligand was never successfully isolated and characterized during the few months spent on this project, another member of the Jenkins group picked up the project when he joined the group in January 2015.

Table 4.1. Summary of conditions employed to prepare TIPS-protected thiol.

Entry	Solvent/ volume	Catalyst Load	Temp.	Time
1	toluene/ 1.5 mL	0.025 mol %	110 °C	4 h
2	toluene/ 3 mL	0.025 mol %	110 °C	20 h
3	toluene/ 3 mL	1.25 mol %	110 °C	4 h
4	toluene/ 5 mL	0.025 mol %	110 °C	4 h
5	toluene/ 3 mL	No catatyst	110 °C	22 h
6	tetrahydrofuran	0.025 mol %	65 °C	150
7	benzonitrile	0.025 mol %	110 °C	150
8	acetonitrile	0.025 mol %	85 °C	150
9	o-xylene	0.025 mol %	135 °C	150
10	1,4-dioxane	0.025 mol %	100 °C	150
11	1,2-dimethoxyethane	0.025 mol %	85 °C	80
12	p-xylene	0.025 mol %	135 °C	80
13	mesitylene	0.025 mol %	155 °C	4 h

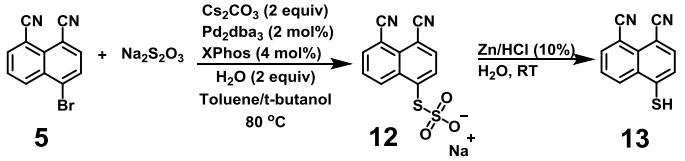

Scheme 4.4. Coupling and deprotection conditions to form aromatic thiol from Bunte salt intermediate.

Experimentals

Synthesis of 5-bromoacenaphthylene-1,2-dione (2). Molecule **2** was prepared according to previously reported procedures.[15] To a clean, dry 250 mL round bottom flask, 15.06 g (0.0827 mol) acenaphthenequinone and 35 mL (108.5 g, 1.36 mol) bromine were refluxed for two hours, then cooled to room temperature, and the bromine was quenched with slow addition of around 150 mL saturated sodium thiosulfate solution. The red-brown solid was filtered and rinsed with around 200 mL water, split into four batches and recrystallized from toluene to afford the pure, yellow product. (15.3 g, 71% yield). ^{1}H NMR (DMSO-d_6, 499.74 MHz): σ 8.39 (d, 1H), 8.21 (d, 1H), 8.15 (d, 1H), 8.04 (t, 1H), 7.96 (d, 1H). ^{13}C (DMSO-d_6, 125.67 MHz): σ 186.79, 186.60, 144.30, 131.95, 130.56, 130.08, 129.67, 129.49, 128.86, 126.46, 122.11. Not all carbons were observed as it appeared the peak at 122.11 was actually two peaks stacked on top of each other. IR: 1744, 1723, 1604, 1573, 1475, 1422, 1261, 1203, 1164, 1082, 1017, 942, 896, 845, 818, 794, 765, 719 cm^{-1}.

Synthesis of 3-bromoacenaphtho[1,2-c][1,2,5]thiadiazole 8,8-dioxide (4). Molecule **4** was prepared according to previously reported procedures.[12] To a clean, dry 250 mL round bottom flask, 4.50 g (17.2 mmol) 5-bromoacenaphthylene-1,2-dione and 3.34 g suflamide (34.8 mmol) and flushed with N_2 for 15 minutes. The two reagents were dissolved in 85 mL methanol and heated to reflux. The mixture was stirred for 5 minutes before the slow addition of 12 mL (13.4 g, 0.171 mol) acetyl chloride, after which the reaction turned from a yellow suspension to a clear, orange solution. After a few more

minutes a yellow precipitate formed and the suspension was left to reflux for 12 hours. After cooling to room temperature the reaction mixture was diluted with diethyl ether, filtered over a frit, and the yellow solid was washed 3 more times with ether and left to dry in air. (4.40 g, 80% yield). ^{1}H NMR (DMSO-d_6, 499.74 MHz): σ 8.55 (d, 1H), 8.47 (d, 1H), 8.35 (dd, 2H), 8.16 (t, 1H). ^{13}C (DMSO-d_6, 125.67 MHz): σ 166.6, 166.1, 149.1, 133.8, 132.1, 131.1, 130.7, 128.1, 127.7, 126.9, 123.9, 122.6 ppm. IR: 1632, 1558, 1472, 1409, 1350, 1172, 1101, 1065, 1027, 966, 944, 849, 822, 801, 784, 760, 752, 701, 671, 652, 634 cm^{-1}. DART/MS (*m/z*): $[M+H]^+$ 320.9 (found), 319.9 (calculated).

Synthesis of 4-bromonaphthalene-1,8-dicarbonitrile (5). Molecule **5** was prepared according to previously reported procedures.[12] To a clean, dry 250 mL round bottom flask, 4.38 g (13.6 mmol) 3-bromoacenaphtho[1,2-c][1,2,5]thiadiazole 8,8-dioxide was dissolved in 125 mL diethyl glyme and heated to 200 °C. The mixture turned to a dark brown suspension and SO_2 could be observed evolving out of solution as white gas. The reaction stirred for a total of 20 minutes at this temperature before immersing flask in ice, diluting with hexanes, and cooling to 0 °C over 1 h. The solid was filtered, rinsed with hexanes, the pentane, and dried under high vacuum overnight. The product could be further purified by recrystallization from hot toluene. (2.91 g, 83% yield). ^{1}H NMR (DMSO-d_6, 499.74 MHz): σ 8.67 (d, 1H), 8.48 (d, 1H), 8.26 (dd, 2H), 7.99 (t, 1H). ^{13}C (DMSO-d_6, 125.67 MHz): σ 139.8, 138.8, 134.0, 132.0, 131.7, 130.3, 129.4, 129.3, 116.7, 116.7, 108.5, 107.8 ppm. IR: 2221, 1564, 1504, 1391, 1368, 1231, 1043, 985, 838, 813, 785, 759 cm^{-1}. DART/MS (*m/z*): $[M+H]^+$ 256.98 (found), 256.96 (calculated).

References

1. Bunn, G., The Nuclear Nonproliferation Treaty: History and Current Problems. *Arms Control Today* December 2003.
2. Kristensen, H. M.; Norris, R. S., Slowing nuclear weapon reductions and endless nuclear weapon modernizations: A challenge to the NPT. *B. Atom. Sci.* **2014,** *70*, 94-107.
3. International Atomic Energy Agency. https://www.iaea.org/safeguards (accessed March 30, 2016).
4. Boulyga, S. F., Becker J. S., Isotopic Analysis of Uranium and Plutonium Using ICP-MS and Estimation of Burn-Up of Spent Uranium in Contaminated Environmental Samples. *J. Anal. At. Spectrom.* **2002,** *17*, 1143-1147.
5. Weaver, M., FBI foils plot to sell nuclear material in Moldova. *The Guardian* 2015.
6. Gordon, M. R.; Sanger, D. E., Deal Reached on iran Nuclear Program; Limits on Fuel Would Lessen With Time. *The New York Times* 2015.
7. (a) Arockia Jency, D.; Umadevi, M.; Sathe, G. V., SERS detection of polychlorinated biphenyls using β-cyclodextrin functionalized gold nanoparticles on agriculture land soil. *J. Raman Spectrosc.* **2015,** *46*, 377-383; (b) Tira, D.-S.; Potara, M.; Astilean, S., Fabrication of stable network-like gold nanostructures in solution and their assessment as efficient NIR-SERS platforms for organic pollutants detection. *Mater. Res. Bull.* **2015,** *64*, 267-273; (c) Wei, H.; Hossein Abtahi, S. M.; Vikesland, P. J., Plasmonic colorimetric and SERS sensors for environmental analysis. *Environ.Sci. Nano* **2015,** *2*, 120-135.
8. (a) Beier, H.; Cowan, C.; Chou, I. H.; Pallikal, J.; Henry, J.; Benford, M.; Jackson, J.; Good, T.; Coté, G., Application of Surface-Enhanced Raman Spectroscopy for Detection of Beta Amyloid Using Nanoshells. *Plasmonics* **2007,** *2*, 55-64; (b) Grubisha, D. S.; Lipert, R. J.; Park, H.-Y.; Driskell, J.; Porter, M. D., Femtomolar Detection of Prostate-Specific Antigen: An Immunoassay Based on Surface-Enhanced Raman Scattering and Immunogold Labels. *Anal. Chem.* **2003,** *75*, 5936-5943; (c) Shafer-Peltier, K. E.; Haynes, C. L.; Glucksberg, M. R.; Van Duyne, R. P., Toward a Glucose Biosensor Based on Surface-Enhanced Raman Scattering. *J. Am. Chem. Soc.* **2003,** *125*, 588-593; (d) Shi, C.; Zhang, Y.; Gu, C.; Seballos, L.; Zhang, J. Z. In *Low concentration biomolecular detection using liquid core photonic crystal fiber (LCPCF) SERS sensor*, 2008; pp 685204-685204-8; (e) Yonzon, C. R.; Haynes, C. L.; Zhang, X.; Walsh, J. T.; Van Duyne, R. P., A Glucose Biosensor Based on Surface-Enhanced Raman Scattering: Improved Partition Layer, Temporal Stability, Reversibility, and Resistance to Serum Protein Interference. *Anal. Chem.* **2004,** *76*, 78-85.
9. (a) Bernstein, K. J.; Do-Thanh, C.-L.; Penchoff, D. A.; Alan Cramer, S.; Murdock, C. R.; Lu, Z.; Harrison, R. J.; Camden, J. P.; Jenkins, D. M., The synthesis and spectroscopic characterization of an aromatic uranium amidoxime complex. *Inorg. Chim. Acta* **2014,** *421*, 374-379; (b) Kristo, M. J.; Tumey, S. J., The state of nuclear forensics. *Nuc. Instrum. Methods Phys. Res. Sect. B* **2013,** *294*, 656-661.

10. Sharma, B. F., R. R.; Henry, A. I.; Ringe, E.; Van Duyne, R. P., SERS: Materials, applications, and the future. *Mater. Today* **2012,** *15*, 16-25.
11. (a) Fan, M.; Andrade, G. F. S.; Brolo, A. G., A review on the fabrication of substrates for surface enhanced Raman spectroscopy and their applications in analytical chemistry. *Anal. Chim. Acta* **2011,** *693*, 7-25; (b) Kneipp, K.; Wang, Y.; Kneipp, H.; Perelman, L. T.; Itzkan, I.; Dasari, R. R.; Feld, M. S., Single Molecule Detection Using Surface-Enhanced Raman Scattering (SERS). *Phys. Rev. Lett.* **1997,** *78*, 1667-1670; (c) Le Ru, E. C.; Blackie, E.; Meyer, M.; Etchegoin, P. G., Surface Enhanced Raman Scattering Enhancement Factors: A Comprehensive Study. *J. Phys. Chem. C* **2007,** *111*, 13794-13803; (d) Nie, S.; Emory, S. R., Probing Single Molecules and Single Nanoparticles by Surface-Enhanced Raman Scattering. *Science* **1997,** *275*, 1102-1106.
12. Grant, C. D.; Kang, S. O.; Hay, B. P., Synthesis of a Hydrophilic Naphthalimidedioxime. *J. Org. Chem.* **2013,** *78*, 7735-7740.
13. Fernández-Rodríguez, M. A.; Hartwig, J. F., One-Pot Synthesis of Unsymmetrical Diaryl Thioethers by Palladium-Catalyzed Coupling of Two Aryl Bromides and a Thiol Surrogate. *Chem. Eur. J.* **2010,** *16*, 2355-2359.
14. (a) Lee, M.-T.; Hsueh, C.-C.; Freund, M. S.; Ferguson, G. S., Electrochemical Self-Assembly of Monolayers from Alkylthiosulfates on Gold. *Langmuir* **2003,** *19*, 5246-5253; (b) Lukkari, J.; Meretoja, M.; Kartio, I.; Laajalehto, K.; Rajamäki, M.; Lindström, M.; Kankare, J., Organic Thiosulfates (Bunte Salts): Novel Surface-Active Sulfur Compounds for the Preparation of Self-Assembled Monolayers on Gold. *Langmuir* **1999,** *15*, 3529-3537.
15. Wang, L.; Wang, X.; Cui, J.; Ren, W.; Meng, N.; Wang, J.; Qian, X., Preparation of chiral trans-5-substituted-acenaphthene-1,2-diols by baker's yeast-mediated reduction of 5-substituted-acenaphthylene-1,2-diones. *Tetrahedron: Asymmetry* **2010,** *21*, 825-830.

CHAPTER 5
CONCLUSIONS

Chapter Summaries

MONTs are the 1D variant of MOFs and hold promise as an emerging 1D material because of its intrinsic chemical tunability derived from the organic portion of the material. Because chemists and engineers can fine tune features like pore size, chemical environment, and metal valency, MONTs offer a unique alternative to purely organic and inorganic nanotubes that are limited to a narrow pore diameter and elemental composition. It is critical to develop methods to prepare discrete MONTs in order to harness its properties as a highly anisotropic, metal-organic hybrid, 1D material.

Our initial attempts to post-synthetically disperse a Ag MONT that our group previously reported, and characterize the discrete nantubes using TEM were unsuccessful. Our follow-up work to image the packed MONTs were hindered by sample amorphization under the electron beam in spite of attempts to control the voltage and current. Our collaboration with the Dadmun group, however, offered more fruitful results where we were able to study the reaction kinetics and growth of the Ag nanotube $[Ag_2(\mathbf{1})(NO_3)_2]$•NMP. SAXS allowed us to determine that the nanotubes form initial isotropic stuctures, then undergo an autocatalytic 1D chain growth to form the tube. A complementary SEM study revealed nanorods early in the reaction, and nanobuds were observed on the surface of these rods, indicative of nucleation sites for crystal growth. The data was modeled to fit the Gualtieri method of nucleation and growth, which was developed for the solvothermal synthesis of zeolites, and the data best fit when the variable of dimensionality was set to 1, indicating 1D rods. Future SAXS work will focus

on generalizing this study to other MONTs prepared in our group as well as literature MONTs, fused tubes, and 2D sheet MOFs in order to determine if SAXS is a good method to characterize discrete nanotubes, or bundles of a handful of tubes.

Synthetic work during my tenure at the University of Tennessee focused on ligand design, specifically ligands that will allow for pore height and width to be altered independently, and functionalized ligands that will inhibit MONT aggregation *in situ*. Initial work to synthesize extended linkers was unsuccessful largely because the ligands involved in the cross coupling reactions were insufficient to overcome the activation barrier. One new synthon was prepared, 4-(4-(4,4,5,5-tetramethyl-1,3,2-dioxaborolan-2-yl)phenyl)-4H-1,2,4-triazole, but the triazole portion of the molecule most likely coordinated to the palladium and inhibited initiation of the catalytic cycle. Our focus later shifted from preparing extended linkers to ones that are functionalized in order to inhibit nanotube aggregation as they form. For samples prepared in the Jenkins group, MONT aggregation is driven by π-π stacking and it was presumed that incorporation of functional groups of varying size and steric bulk would mitigate this problem. Initial work focused on alkyl-ether functionalized ligands starting with the *meta* and *para* isomers of dimethylphenol, bromination with NBS, then carrying out the remaining two steps modified from Horváth's procedure. This sequence was hindered by purification of the bromination product, and only in one case was I able to isolate product pure enough to continue the sequence. The low yields and poor reproducibility prevented large scale synthesis of the ligand. Focus to exclusively ligands functionalized with alkyl groups, but

the same problem was encountered. Future work, currently being carried out by Kristina Vailonis, is exploring alternative bromination paths that will be much easier to purify.

A tetrazole analog of the *para*-ditriazole ligand employed by Christopher Murdock was synthesized with help from a former undergraduate member of our group, Khanh Pham. The ligand was prepared at the 8 g scale and was readily purified by extraction with 1M KOH, filtration, and acidification. Test reactions were carried out in numerous solvent combinations and in pH conditions ranging from 2 to 8. Most of the samples resulted in the formation of gels, and acidic conditions exacerbated this problem. Five powder crystalline samples were synthesized from $AgNO_3$ or $CuSO_4 \cdot 6H_2O$, but of these, only two samples prepared from $CuSO_4$ were reproducible. IR spectra verified that the ligand was indeed bound to the metal but no structural information was elucidated. SEM images were obtained of the two reproducible samples and needle-like nanorods were observed, indicating potential nanotube formation, but the connectivity remains unknown. Several single crystalline samples were obtained from reaction of $CuSO_4$ and the tetrazole ligand in pyridine with addition of a small volume of acid, but each revealed the same structure: a 2D coordination polymer that stacked in layers to form the 3D crystal. Altering the solvent to pyridine derivatives, 2,6-picoline and 2,6-lutidine, failed to result in successful reactions due to poor solubility of the ligand in these solvents. Future work should focus on carrying out these reactions in basic, aqueous solutions as deprotonation of the ligand enhances its solubility in water.

Nuclear detection is a field that has important applications in global security and environmental remediation. The ability to develop a portable device that can accurately

detect the presence, quantity, and isotope of a given radionuclide will be an invaluable technology with far reaching applications. Synthetic work during my first year in graduate school focused on preparing a thiol-functionalized cyclic amidoxime ligand to employ in a SERS-based portable Raman spectrometer that can be used for on-site nuclear forensics.

I was able to successfully synthesize two key intermediates in high yield at the multi-gram scale, I was unable to prepare the aromatic thiol by way of a cross-coupling reaction with triisopropylsilanethiol developed by Hartwig and company. Numerous solvent and temperature conditions were studied, and despite observing the product in the DART mass spectrometer, the product was never able to be isolated. Joseph DeJesus has taken over the project and found alternative synthetic routes that have been more fruitful for preparing new ligands to study.

Thesis Summary

Metal-organic nanotubes are an emerging class of porous materials that are the 1D variant of metal-organic frameworks. Most MONTs reported to date are packed in 3D crystalline lattices, and thus methods are required to disperse them to their discrete form in order to harness the unique properties that are dependent upon a material's dimensionality. The work detailed in this thesis formed the basis for future work for developing methods to facilitate this dispersion, like employing novel anionic ligands and ligands functionalized with bulk groups that inhibit the aggregation as they form. Though challenges were encountered in the synthesis of new ligands, the overarching theme of

this thesis underscores the element of rational design in coordination materials, a feature that has helped to propel synthetic porous materials to the forefront of the scientific community. Additional work is required that will enable thorough characterization of discrete materials that exist at the sub-nanometer regime, rather than rely on bulk characterization using X-ray crystallography.

Potential Future Directions

A general method to characterize MONTs with SAXS is imperative for characterization. SAXS is an indirect method and thus relies on complementary studies, like SEM or TEM, in order to thoroughly understand the system in question. A study that evaluates multiple coordination materials, including 3D or 2D MOFs, and other literature MONTs in order to understand how growth and kinetics change from system to system. It is important to understand how the different classes of MONTs form, how they differ from each other, and if the Gualtieri model be extended to other structures composed of much simpler ligands. Further understanding the mechanistic and kinetic differences between the formation of discrete and bulk materials will be invaluable information to guide researchers to design new, more robust MONT systems.

Ligand design is becoming increasingly important in MOF and MONT synthesis and requires efficient routes to prepare what can be complex structures. Synthesis of new semi-rigid di-triazole and di-tetrazole ligands should employ simple reactions that require minimal purification, a step that can often impede progress. For example, NBS has been a valuable bromination reagent in the chemical literature, multiple brominations

products form when brominating more than one carbon in a single step. Evaluating other routes to prepare the di-brominated intermediates will be crucial to synthesize new di-triazole ligands.

Coupling reactions have been invaluable for other groups and employing aryl-alkyl coupling reactions to functionalize the aromatic backbone should be properly investigated as this could be a simple way to design a large library of ligands rather than rely on commercially available synthons that can be expensive. Additionally, coupling reactions will be necessary to form ligands that allow pore height and width to be properly tuned. Catalytic systems that are tolerant of a wide range of functional groups will be necessary as the ligands our group employs rely on *N*-heterocyles, which are typically incompatible with most standard catalytic reactions.

Finally, appropriate conditions for which the tetrazole can bind to the metal will be necessary to explore. Because the tetrazole can form an anion in solution, it is likely this will form a MONT that does not require counter anions or counter cations within the pore, thus leaving the interior of the framework free for storage, transfer, or separations. Aqueous, basic solutions have prevented gel formation and will serve as a good starting point for new MONT discovery. A range of bases should be evaluated, including hydroxide, alkoxide, and organic bases like trimethylamine, pyridine, and others.

VITA

Derek Lowell Mull was born on August 4, 1988 in Wauseon, Ohio to Linda and Kevin Mull. He was raised in neighboring Delta, Ohio, where he graduated from Pike-Delta-York Senior High school in 2006, then received a scholarship to attend the University of Toledo where he studied biology and chemistry. During his time at Toledo, he was a member of the Honors College, numerous student organizations, and participated in a one academic year exchange program at the University of Salford in the Greater Manchester region in the UK where he studied biochemistry and molecular biology. After returning to Toledo, he worked under Dr. Cora Lind to synthesize metastable phases of tantalum sulfide using non-hydrolytic sol gel chemistry, and completed his honors thesis under her direction. He earned his bachelor's degree in biology and chemistry with university and departmental honors in 2011.

During his final semester at Toledo and the summer following graduation, Derek participated in the Higher Education Research Experience (HERE) program at Oak Ridge National Laboratory (ORNL) in Tennessee and where worked with Dr. Claudia Rawn and her graduate student Dr. S. Michelle Everett to study the kinetic decomposition of methane clathrate hydrates as part of a DOE funded alternative energy project. After his time at ORNL, Derek relocated to Los Angeles, CA to work under Dr. Omar M. Yaghi where he worked on a few MOF synthesis projects. It was during this time that Derek developed his understanding of MOFs, their applications, and immersed himself in the literature.

Following a year break from academia, Derek moved back to Knoxville to begin his graduate studies at the University of Tennessee, Knoxville (UTK) under Dr. David Jenkins to synthesize discrete metal-organic nanotubes. Derek began working for Dr. Jenkins the summer before he began graduate school, and chose to join the Jenkins group early on his first semester. Derek won the prestigious National Science Foundation Graduate Research Fellowship in 2014, the first chemistry student at UTK to win the award in 21 years.